SERI/TR-255-2217
DE84004518

May 1984

Materials Characterization Using Ion, Electron, and Photon Probes

A. W. Czanderna

SERI

Solar Energy Research Institute
A Division of Midwest Research Institute

1617 Cole Boulevard
Golden, Colorado 80401

Operated for the
U.S. Department of Energy
under Contract No. DE-AC02-83CH10093

Printed in the United States of America
Available from:
National Technical Information Service
U.S. Department of Commerce
5285 Port Royal Road
Springfield, VA 22161
Price:
Microfiche A01
Printed Copy A04

NOTICE

This report was prepared as an account of work sponsored by the United States Government. Neither the United States nor the United States Department of Energy, nor any of their employees, nor any of their contractors, subcontractors, or their employees, makes any warranty, express or implied, or assumes any legal liability or responsibility for the accuracy, completeness or usefulness of any information, apparatus, product or process disclosed, or represents that its use would not infringe privately owned rights.

SERI/TR-255-2217
UC Categories: 59, 61c, 62, 63d,e, 64
DE84004518

Materials Characterization Using Ion, Electron, and Photon Probes

A. W. Czanderna

May 1984

Prepared under Task No. 1064.10
FTP No. 117-84

Solar Energy Research Institute
A Division of Midwest Research Institute

1617 Cole Boulevard
Golden, Colorado 80401

Prepared for the
U.S. Department of Energy
Contract No. DE-AC02-83CH10093

PREFACE

The purpose of this report is to document the content of a lecture prepared for a Distinguished Lecture Series in Industrial Materials Science at the Oregon Graduate Center, Beaverton, Oregon. During the fall of 1983, students at the Lecture Series received graduate credit for attending twelve lectures on various topics in industrial materials science. The emphasis of my lecture was materials characterization using ion, electron, and photon probes and the intended level was for undergraduate seniors and beginning graduate students. The content of this report is one of the chapters in the book Industrial Materials Science and Engineering, L. E. Murr (ed.). Dekker, N.Y., 1984 in which written versions of the entire Distinquished Lecture Series are also published.

I am grateful to Dr. L. E. Murr for inviting me to participate in the program. I also acknowledge with thanks J. R. Pitts, T. M. Thomas, and J. D. Webb of the Materials Research Branch at the Solar Energy Research Institute with whom I have been privileged to collaborate on securing several of the research results used as examples in this report.

The support of the Department of Energy, Office of Energy Research, Basic Energy Sciences, Division of Materials Sciences is gratefully acknowledged. This work was performed under DOE Contract No. DE-AC02-83CH10093.

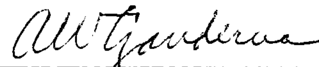

A. W. Czanderna, Research Fellow

Approved for

SOLAR ENERGY RESEARCH INSTITUTE

Gordon E. Gross, Chief
Materials Research Branch

L. J. Shannon, Director
Solar Heat Research Division

SUMMARY

Objective

To introduce the reader to using ion, electron, and ion probe beams as methods of compositional analysis in materials characterization.

Discussion

These beams can provide information about the compositional, chemical state, and lateral distribution of the outer few atomic layers of solid surfaces. The closely related topical areas in surface science of topography, structural surface analysis, and deducing chemical bonding information at the solid/gas or solid/vacuum interface are not discussed. There are three major sections dealing with compositional surface analysis, i.e., composition in-depth profiling, commercially available methods of surface analysis, and typical applications.

The depth distribution of elements into a solid may be determined by composition in depth profiling. Surface sensitive probe beams are used for securing the elements present on the surface, and ion etching is used to expose the subsurface atomic layers of a material. The principal advantage of the ion etching method is that near atomic depth resolution is possible, in principle. The principal disadvantage is that the energetic ion bombardment introduces artifacts that complicate the analysis.

Compositional surface analysis may be performed using ion beams, such as secondary ion mass spectrometry (SIMS), ion scattering spectrometry (ISS), or Rutherford backscattering spectrometry (RBS); electron beams such as Auger electron spectroscopy (AES); or photon beams such as X-ray photoelectron spectroscopy (XPS). Each of these five methods is commercially available and has specific advantages and limitations. The outstanding advantages include high sensitivity for SIMS, monolayer sensitivity for ISS, quantitative and non-destructive analysis for RBS, lateral resolution for AES, and chemical state information for XPS. The significant limitations include difficulty in quantification in SIMS, poor resolution for high Z elements for ISS and RBS, electron beam damage and electron stimulated desorption for AES, and long data acquisition times for XPS that limit its usefulness for depth profiling.

Conclusions

The methods of elemental surface analysis, SIMS, ISS, RBS, AES, and XPS have been applied to a wide variety of problems in materials science and engineering. These problems are in such diverse topical areas as corrosion, surface segregation, surface modification, photovoltaic materials, interdiffusion, glasses, polymers, and solar mirrors. Compositional analysis can be routinely performed on metals, semiconductors, insulators, ceramic, glassy, and polymeric materials, but not all materials can be successfully probed with all techniques.

TABLE OF CONTENTS

	Page
1.0 Introduction	1
2.0 Composition-In-Depth Profiling	3
2.1 Sputtering Mechanism, Yield, and Rate	3
2.2 Instrumentation	7
2.3 Data Obtained and Typical Results	8
3.0 Compositional Surface Analysis	11
3.1 Secondary Ion Mass Spectrometry (SIMS)	12
3.1.1 Physical Principles and Processes	12
3.1.2 Experimental	13
3.1.3 Advantages and Limitations of SIMS	15
3.2 Ion Scattering Spectrometry (ISS)	17
3.2.1 Physical Principles and Scattered Ion Yield	17
3.2.2 Experimental	19
3.2.3 Major Advantages and Limitations of ISS	20
3.3 Rutherford Backscattring Spectrometry (RBS)	22
3.3.1 Physical Principles	22
3.3.2 Experimental	23
3.3.3 Advantages and Limitations of RBS	26
3.4 X-Ray Photoelectron Spectroscopy (XPS)	26
3.4.1 Physical Principles	27
3.4.2 Experimental	30
3.4.3 Advantages and Limitations of XPS	30
3.5 Auger Electron Spectroscopy (AES)	31
3.5.1 Physical Principles	32
3.5.2 Experimental	33
3.5.3 Advantages and Limitations of AES	34
4.0 Applications of Surface Compositional Analysis	36
4.1 Surface Modification of Materials	36
4.2 Surface Segregation and Interdiffusion	36
4.3 Corrosion	36
4.4 Photovoltaic Materials and Interfaces	37
4.5 Glasses	37
4.6 Polymers	37
4.7 Solar Mirrors	39
5.0 References	41

LIST OF FIGURES

		Page
2-1	Ideal and Experimental Depth Profiles for Thin Film Multilayers....	4
2-2	Objectives and Practice of Depth Profiling. The Objective of Atomic Layer Microsectioning Cannot be Achieved because of the Gaussian Shape of the Ion Intensity................................	5
2-3	Several of the Possible Collision Processes that Occur During Ion Bombardment. Surface Atoms Are Ejected from Being Hit from (1) Above or (2) Below; Some Do Not Receive Enough Energy to Leave the Surface (3) or Leave and Fall Back (4). Occasionally, Bulk Atoms Receive Enough Energy to Escape (5); Others, (6) Simply Receive Energy..	6
2-4	Schematic of an Ion Gun for a Primary Beam. The Mass Separator and Scanning Units are Optional, as Indicated by the Brackets (see Ref. 10)..	8
2-5	Depth Profiles of Boron Ion Implanted (at 150 keV) into Silicon Using Different Methods to Improve the Quality of the Measured Profile (see Ref. 20)..	9
2-6	^{18}O Depth Profile in a Ta_2O_5 Sample Used to Evaluate Depth Resolution. The Center 100 nm of the Film was Enriched with ^{18}O. The 16% and 84% Points of the Signal Level Represent ±1 Standard Deviation from the Half Maximum Value and Serve to Evaluate Depth Resolution. The Detected Ion was $^{18}O^-$ (see Ref. 20)..	10
3-1	Generalized Input and Output Probes for Surface Analysis. The Electron Energy (AES, XPS), Ion Energy (ISS, RBS), and Ion Mass (SIMS) Are the Measured Output Parameters.....................	11
3-2	Principle of SIMS (see Ref. 10)..................................	14
3-3	SIMS Spectrum of a Silver Standard................................	16
3-4	Schematic Representation of the Scattering of a Projectile Ion from a Surface Atom and the Recoil of the Surface Atom M_2 with the Energy E_2..	18
3-5	ISS Spectra for (a) Polypropylene, (b) $Cu^{18}O_{0.67}$ Film at the Oxide/Glass Interface, (c) $Cu^{18}O_{0.67}$ Film at the Oxide/Pt Interface, and (d) $Cu^{18}O_{0.67}$ Film at the Oxide/Au Interface (see Ref. 91).....	21
3-6	Schematic Representation of the Scattering of Projectile Ions from Surface and Bulk Atoms of M_2 and Z_2 Through a Scattering Angle ρ to Form an RBS Spectrum (see Ref. 40)......................	23

LIST OF FIGURES (Concluded)

Page

3-7 The Height H_i of the Ion Yield with Energies of ΔE from MeV Ion Scattering from Bulk Atoms of Thickness t_i at a Depth of X_i (see Ref. 40) 25

3-8 RBS Spectra for Scattering from a High Z Material on a Low Z Material and Vice Versa (see Ref. 40) 25

3-9 Electron Energy Levels for Aluminum Showing Ejection of 2s, 2p, or Valence Band Electrons by Photons to Produce the Intensity Shown in an XPS Spectra of N(E) vs. Binding Energy 27

3-10 An EPS Survey Spectrum Showing the Presence of Ag, O, Sn, Ca, Na, Si, and C at the Silver-Glass Interface of a Mirror after Etching through 70 nm of Silver Deposited onto a Sensitized Glass Substrate (see Ref. 91) 28

3-11 The Atomic Sensitivity of Strong Lines in XPS Spectra vs. the Atomic Number 29

3-12 The Mean Escape Depth of Ejected Electrons vs. Energy (see Ref. 45) 29

3-13 Electron Energy Levels for Aluminum Showing Ejection of a K or an L Electron by Incident Electrons to Produce the KLL or LMM Auger Electron Intensity in a Spectrum of N(E) vs. Electron Energy 33

3-14 Peak to Peak Amplitude from dN(E)/dE vs. E Auger Spectra Taken during a Depth Profile through the Copper Layer of a One Year Old Mirror after Removal of a Lacquer Backing with Acetone. The Profile Has Been Corrected for Elemental Sensitivity Factors as Provided by Physical Electronics. E_p = 3 keV, I_p = 5 μA, Beam Size ~ 12 μm, E_{Ar+} = 3 keV, 1 mm × 1 mm Raster Area, I_{Ar+} = 200 nA. The Elements Present on the Copper Surface are Shown in the Inset Survey Scan Showing a Plot of dN(E)/dE vs. E (see Ref. 91) 35

4-1 Path of Infrared Radiation through a Controlled Environmental Exposure Chamber for in situ Photodegradation of Polymeric Films on Reflecting Substrates. The Technique Is Known as Reflection-Absorptance Infra-red Spectroscopy and with a Fourier Transform Spectrometer Is Defined as FT-IR-RA (see Ref. 89) 38

4-2 Morphology and Chemical Components Used in a Typical Commercially Made Mirror (see Ref. 91) 40

SECTION 1.0

INTRODUCTION

The purpose of this report is to provide a brief review of characterizing materials by using ion, photon, and electron probe beams. In general, these beams provide information about the surface of solid materials; i.e., the surface is the outer monolayer or the first few atomic layers of the solid. There are a few exceptions where information is obtained from 5 to 100 nm into the solid, and these will be noted when encountered. The probe beams are used in the field of surface analysis; i.e., the regime of surface science dealing with the composition, structure, and bonding of surfaces. Naturally, the chemical entities present and their geometric arrangements influence markedly the electrical, mechanical, optical, magnetic, and stability properties of the materials, so in this sense surface analysis deals with the materials science of surfaces. Of necessity, the beams are generally used in vacuum, so the materials of interest must be stable in a vacuum environment.

The concept of a surface is not well defined, especially for most samples of industrial interest. The structure and composition of a material often deviate from their bulk values for depths of micrometers in a spatially inhomogeneous manner. As is well known [1], each method of surface spectroscopy has its own depth and areal resolution and, therefore, presents its unique view of the inhomogeneous region of the solid. The information available from surface analysis includes identifying the elements present, their lateral distribution, and their depth distribution; in addition, structural and topographical information can also be obtained [2].

Compositional analysis, the primary subject of this report, involves determining three quantities. The elemental identity; i.e., atomic number, is of primary interest. However, it is also desirable to know the chemical state of the species; e.g., elemental, oxidized, or reduced. Finally, it is necessary to determine the spatial distribution of the chemical species. An important trend in compositional surface analysis is the demand for greater and greater lateral resolution; e.g., 50 nm can now be routinely reached using Auger spectroscopy. The study of compositional differences between grains and the grain boundary region is an extremely important area of materials science for deducing how these differences change the materials properties [3].

Structural surface analysis also involves three levels of desired information [2]. For an ideal, atomically flat, single crystal the structure is specified by the geometry in each cell of the surface unit mesh. Real surfaces contain defects, such as dislocations, steps, kinks, ledges, and grain boundaries. Finally, a new trend is emerging for determining local atomic order for a particular chemical species. Determining surface structure is essentially limited to studies of solid-vacuum or solid-gas interfaces. Only minor mention will be made about this subject.

Most studies of chemical bonding at surfaces are related to the solid-gas and solid-liquid interfaces. The latter can only be probed with ion and electron beams with difficulty [4]. The adsorption of gases on solids can be considered a significant branch of surface science. Although adsorption is

involved in many processes of interest to the materials scientist; e.g., corrosion, contamination, and catalysis, the scope of this report would have to be broadened considerably to deal with the use of probe beams for studying phenomena related to adsorption [5]. Similarly, atomistic dynamics and the electronic structure at the solid-vacuum or the solid-gas interfaces are not considered [2], even though ion, electron, and photon probe beams may be used as part of the surface analysis.

The remainder of this report consists of three major sections. Section 2.0 describes the technique of ion etching used to expose the subsurface portion of a material for compositional analysis. Section 3.0 discusses selected methods of compositional surface analysis. Brief descriptions of the physical principles, experimental conditions, advantages, and limitations are given for each method. Illustrative examples or appropriate references are cited for a typical application of a method. Section 4.0 gives applications of one or more methods of surface analysis on subjects of interest in industrial materials science and engineering. Brief comments are made about materials characterization in corrosion, surface modification, surface segregation, thin films, and grain boundaries for ceramic, glass, metallic, organic polymeric, and semiconducting materials.

SECTION 2.0

COMPOSITION-IN-DEPTH PROFILING

Many industrial processes require that the depth distribution of elements be determined. Surface sensitive probe beams can be used for this purpose when combined with the commonly used method of ion etching, which is also known as ion milling, sputter etching, composition-in-depth profiling (CIDP), depth profiling, and (atomic) layer-by-layer microsectioning. An ideal depth profile is shown in Figure 2-1 for a multilayer stack of partially oxidized aluminum on partially oxidized silicon. Sputtering, the process of removing material by bombarding the surface continuously with an energetic ion beam (typically 3 to 10 keV or argon ions), in principle provides a means for atomically microsectioning the solid, and the sputtering time can be related to depth. The principle of microsectioning is shown in Figure 2-2, where it is desired to obtain an analysis at each atomic layer into the solid. As illustrated, the available drill; i.e., an ion beam, produces a Gaussian-shaped crater, so the beam is rastered to remove an area of material that may range from 1 to 100 mm^2. The composition is obtained by analyzing the center of the crater and rejecting signals from the crater walls.

The advantages of sputtering for in-depth analysis are considerable. Physical sputtering is an atomic process, so near-atomic depth resolution is possible, in principle. Depth profiling can be performed in situ in vacuum, which means surface compositional analysis and sputtering can generally be performed simultaneously. When inert gases are used, clean surfaces are produced, and reoxidation or recontamination are avoided. Reasonable erosion rates are achieved; e.g., 0.1 to 100 nm/min, so microsectioning to depths of 1000 to 2000 nm are accomplished within reasonable time periods.

The sputtering process itself, however, introduces limitations to the considerable advantages. A zone of mixing is created from knock-on effects, which broadens the depth resolution. Preferential sputtering may occur, and surface roughness may develop. There is a destruction of structure and chemical states. Bulk and surface diffusion of the target may be enhanced during sputtering. Matrix effects may change the erosion rate as the process proceeds. The sputter gas is implanted into the solid, which is particularly serious when reactive gases such as oxygen or nitrogen are used. Redeposition of sputtered material occurs and complicates the analysis when it occurs on the surface being analyzed. Finally, enhanced adsorption of residual gases in the vacuum occurs, placing more stringent requirements on the vacuum level maintained during in-depth analysis.

2.1 SPUTTERING MECHANISM, YIELD, AND RATE

All current approaches to understanding physical sputtering are based on a model where a sequence of binary elastic collisions occurs (Figure 2-3); i.e., the ion interacts with one target atom at a time [6]. During the multiple collision process, the energy of the incident ion is transferred to lattice atoms until the incident ion is implanted or manages to escape from the solid. H. Winters [6] has discussed the comparison between theory and experiment for

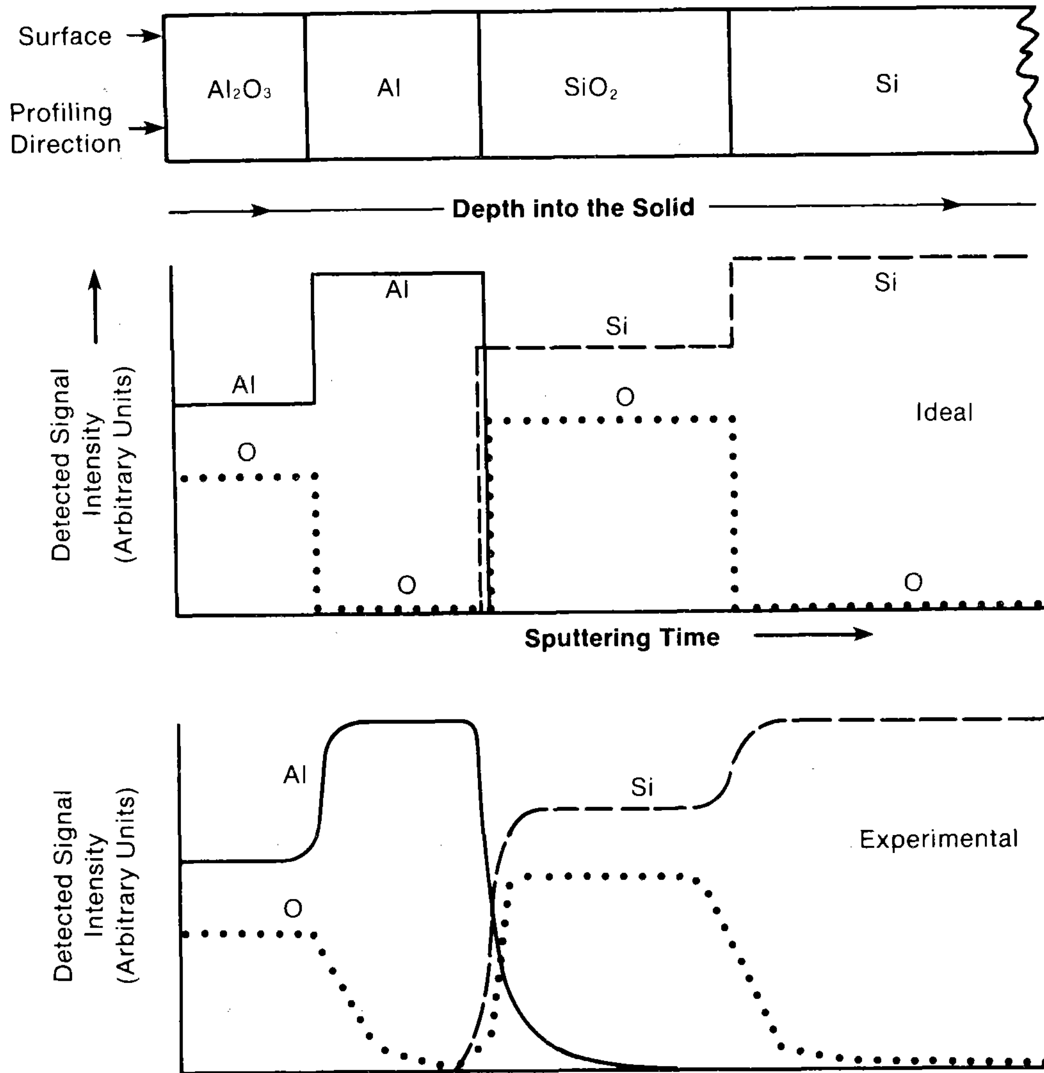

Figure 2-1. Ideal and Experimental Depth Profiles for Thin Film Multilayers

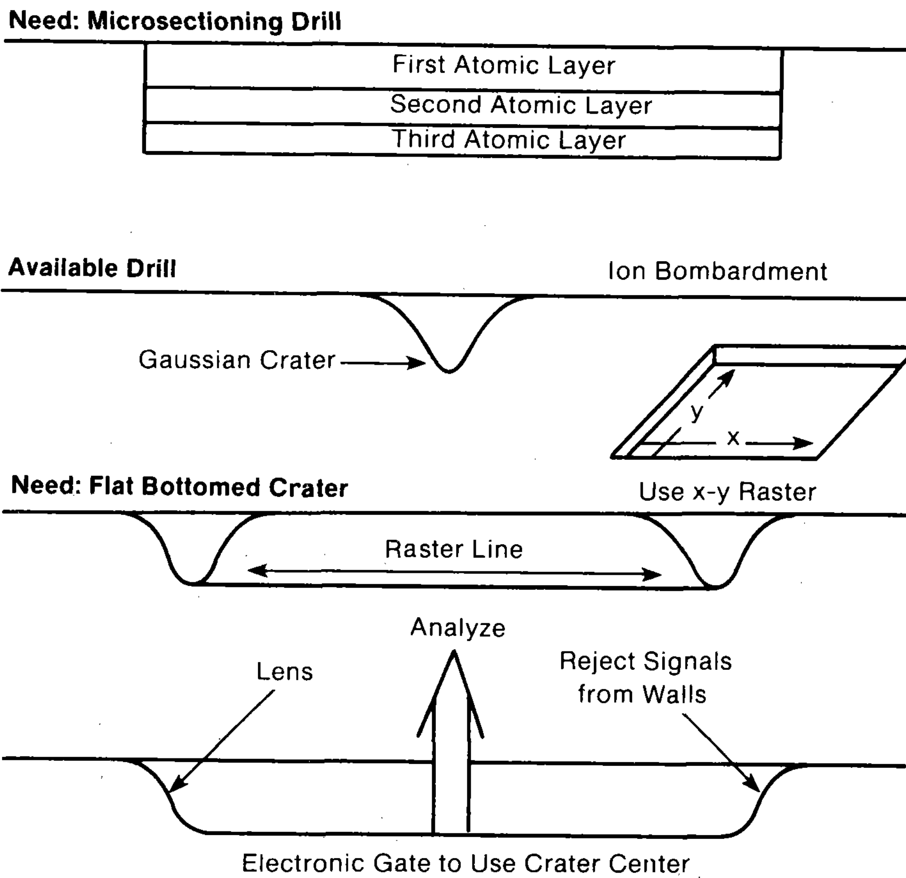

Figure 2-2. Objectives and Practice of Depth Profiling. The Objective of Atomic Layer Microsectioning Cannot Be Achieved because of the Gaussian Shape of the Ion Intensity

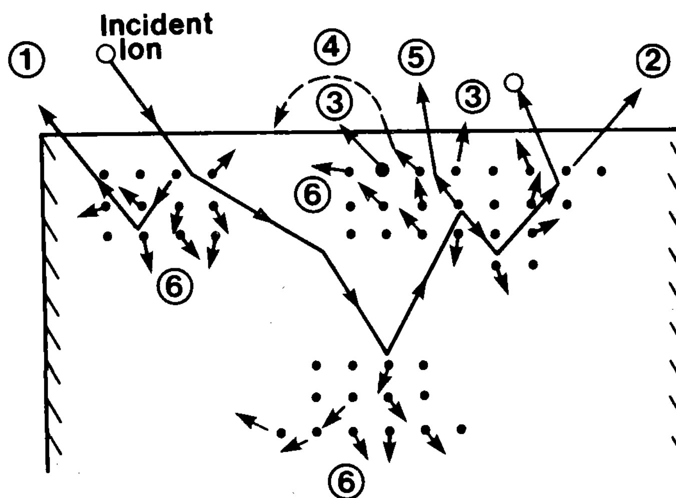

Figure 2-3. Several of the Possible Collision Processes that Occur During Ion Bombardment. Surface Atoms Are Ejected from Being Hit from (1) Above or (2) Below; Some Do Not Receive Enough Energy to Leave the Surface (3) or Leave and Fall Back (4). Occasionally, Bulk Atoms Receive Enough Energy to Escape (5); Others, (6) Simply Receive Energy.

sputtering. As higher energy ions are used, more energy is transferred to the lattice, and the mean escape depth of the target atoms increases [7]. For ideal depth profiling, the mean escape depth should be only from the outer monolayer, which can only be accomplished at low erosion rates. Consequently, to achieve high erosion rates for reaching depths of 10 to 20 μm, the increased amount of energy that must be transferred to the lattice per unit time results in many of the limitations mentioned above. Most of the incident ion energy does not result in ejection of lattice atoms but is transformed into increasing the local temperature of the solid and into the ejection of electrons and photons.

There are many parameters that govern the sputtering yield S, i.e., the number of target atoms ejected per incident ion. Since the binary collision theory is based on the classical mechanics of colliding masses, it is not surprising that the sputtering yield depends on the energy, mass, and angle of incidence of the projectile ion [6,8] as well as the binding energy of the solid [9]. There are other factors that influence the sputtering yield, such as the surface roughness, crystal orientation of the target domains, the electronic properties of the target, the ionization potential of the target, surface cleanliness, residual gases present, and the concentration of implanted ions. Compilations of sputtering yields for commonly used bombardment energies have been made by G. Wehner [8] and H. Werner [10]. For 1-keV noble gas ions at normal incidence onto metal surfaces, S varies from 0.08 for Pt with

the ion bombardment up to 11.2 for Cd under Ar ion bombardment. Variations in S of up to 40 times have been reported for energy ranges of 0.1 to 70 keV; e.g., Ar bombardment of copper.

The erosion or sputtering rate during ion bombardment of solids is given by $dz/dt = 0.006\ SJ^{+}A/\rho$, where dz/dt is in nm/min, S is in atoms per incident ion, J^{+} is the ion beam current density in $\mu A/cm^2$, A is the molecular weight of the target in g/mol, and ρ is the density of the target in g/cm^3 [8]. The erosion rate, which is the time dependent removal of material during ion bombardment, is preferred over sputtering rate, since it is easy to confuse sputtering rate and sputtering yield. According to G. Wehner [8], when using 2 keV Ar ion bombardment at 0.15 mA/cm^2, the erosion rates for stainless steels, Ta, SiO_2, and Ta_2O_5 are in the range of 7 to 13 nm/min; for Pt, the rate is 23 nm/min, while Cu, Au, and Ag are in the range of 30 to 40 nm/min. H. Werner has developed a nomogram relating dz/dt to J^{+} for various values of S at an A/ρ of 10 [10]. He has also published other useful nomograms for selecting various beam parameters and erosion rates as well as for use in secondary ion mass spectrometry.

2.2 INSTRUMENTATION

Depth profiling is accomplished by using a primary ion source; i.e., an ion gun, to direct ions onto the target. A typical ion source is shown schematically in Figure 2-4. A gas is introduced into an ionization chamber at pressures of 10^{-5} to 10^{-1} Pa and is ionized by a discharge process. The ions generated are extracted from the ionization region by using an electric field. After mass separation, which is optional depending on initial gas purity or the desired fidelity of the final beam, the beam is focused to the desired diameter. A Gaussian-shaped beam is typically obtained with the maximum ion intensity on the axis of the beam and the beam diameter stated as the full width at half the maximum (FWHM) intensity of the beam. The stated current density uses the FWHM diameter. It is also important to be aware that ion bombardment occurs on the sample at diminishing intensities at radial distances greater than the FWHM diameter, producing a crater that is approximately an inverted Gaussian shape. To produce a crater with a flat bottom, the ion beam may then be deflected with electric fields to raster the beam over a surface area; e.g., from 2 x 2 mm up to 10 x 10 mm.

Analysis of a part of the flat crater bottom requires two additional modifications of the depth profiling apparatus. One of these is to electronically gate the signal used to identify the elements on the surface and the other is to add a lens that rejects signals from outside the gated area. The quality of the profile is improved by the progression and permutations of using rastering, gating, and an electronic lens as shown in Figure 2-5. Alternative techniques, such as mechanically aperturing the beam or bombarding the surface with a large beam and analyzing with a small beam, are useful when the instrumental capabilities cannot be expanded to include all improvements illustrated in Figure 2-5.

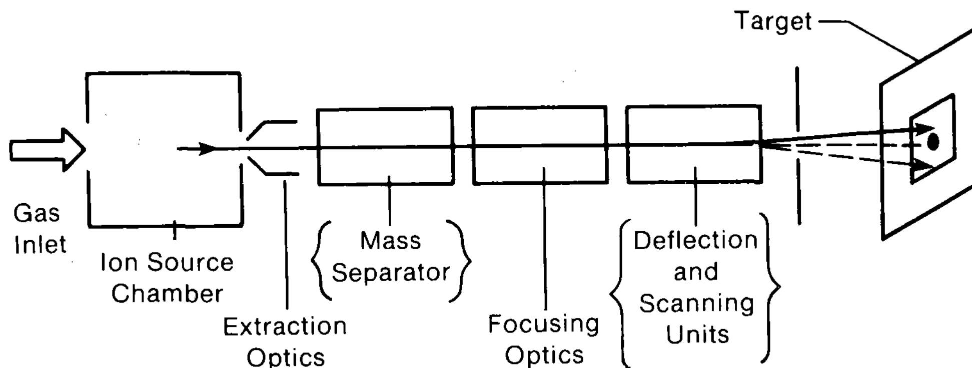

Figure 2-4. Schematic of an Ion Gun for a Primary Beam. The Mass Separator and Scanning Units are Optional, as Indicated by the Brackets (see Ref. 10).

2.3 DATA OBTAINED AND TYPICAL RESULTS

A plot similar to those shown in Figures 2-1 and 2-5 is typically obtained with the abscissa as sputtering time. The conversion of sputtering time to depth can be accomplished by measuring the crater depth after sputtering by using a profilometer; e.g., a stylus instrument for detecting changes in surface topography to about 2.5 nm. An inherent assumption with this method is that the solid was homogeneous and eroded uniformly. For multilayers of pure metals this assumption is usually good, but greater caution must be exercised for multilayers of alloys, oxides, and semiconductors. As a minimum, the erosion rate for each pure material in the multilayer stack must be calibrated.

There are many factors that influence the depth resolution of an interface because of the ion bombardment process. As an example, Figure 2-6 shows the difference in interfacial width in a 300 nm-thick Ta_2O_5 sample, where the middle 100 nm-thick oxide layer was formed in oxygen 18. As is seen, the interface 200 nm deep is broadened more than the one 100 nm thick. This result is generally true, but as yet no simple relationship between interfacial width and depth has been obtained. In fact, there is considerable controversy over possible relationships [11]. The depth resolution depends not only on the quality of the depth profile, but also on factors related to the instrument and the sample. The latter include the basic sputtering process, the original and final sample roughness, ionic mixing, ion transport, knock-in effects, and the incident ion energy.

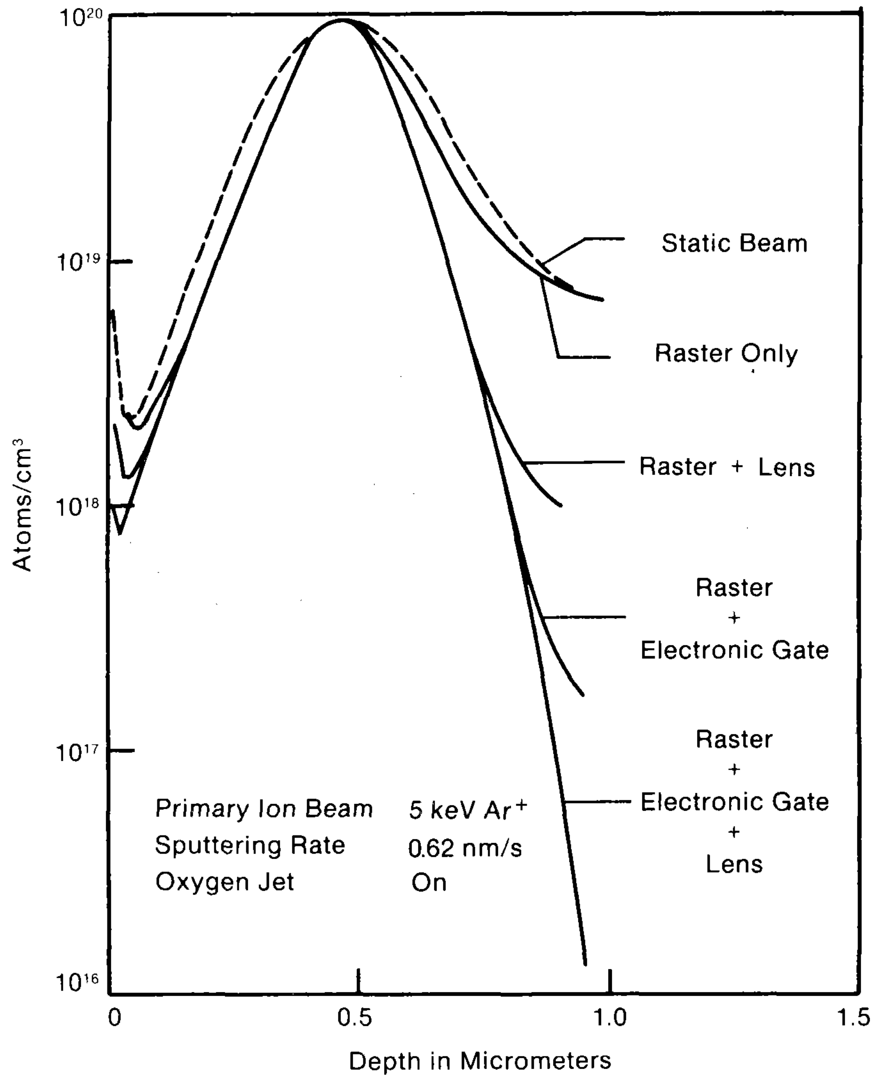

Figure 2-5. Depth Profiles of Boron Ion Implanted (at 150 keV) into Silicon Using Different Methods to Improve the Quality of the Measured Profile (see Ref. 20).

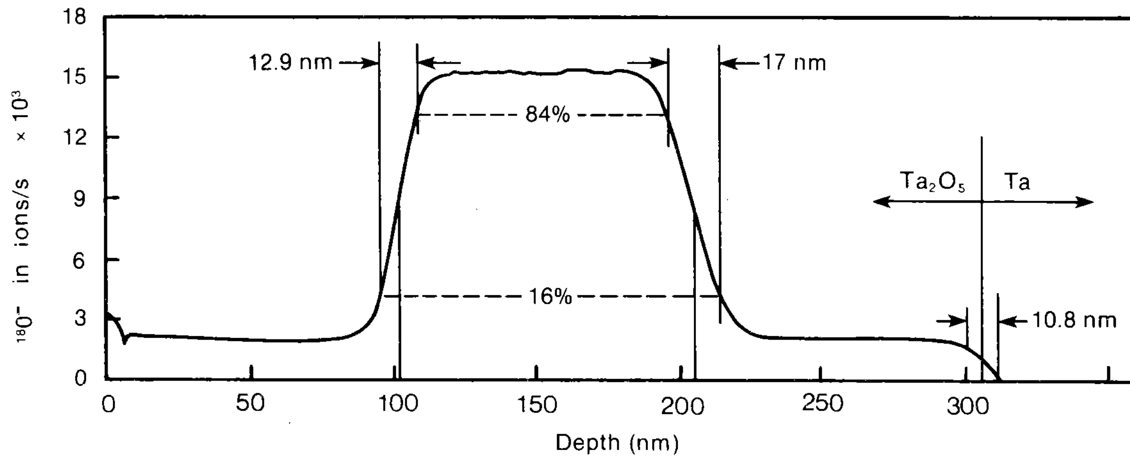

Figure 2-6. ^{18}O Depth Profile in a Ta_2O_5 Sample Used to Evaluate Depth Resolution. The Center 100 nm of the Film was Enriched with ^{18}O. The 16% and 84% Points of the Signal Level Represent ±1 Standard Deviation from the Half Maximum Value and Serve to Evaluate Depth Resolution. The Detected Ion Was $^{18}O^-$ (see Ref. 20).

Examples of artifacts related to limitations of the ion etching process have been illustrated by G. Wehner [8] and P. Holloway and R. Bhattacharya [11]. Artifacts related to the sample include surface roughness, crystallite orientation, lateral variation in impurities from surface diffusion, too great an angle of incidence, matrix effects, and because the surface composition really differs from the bulk. Artifacts resulting because of ion bombardment include ion implantation, amorphization of the surface, enhanced adsorption, enhanced bulk diffusion, knock-in effects, preferential sputtering, cascade mixing, and changes in the chemical states of the target species.

Numerous examples are available of depth profiles taken by various authors using various methods of compositional surface analysis; e.g., see pp. 17, 139, 174, 186, 191, 217, and the chapters by J. McHugh [7] and J. Morabito and R. Lewis [12] in Methods of Surface Analysis edited by A. Czanderna [7]. Additional examples are also available in refs. 4,8,9,10,11.

SECTION 3.0

COMPOSITIONAL SURFACE ANALYSIS

Of the major important parameters for characterizing the gas-solid and solid-solid interface, the most important one is probably the elemental composition [5,13]. A large number of probes have been developed to determine the composition, which is directly related to its importance for the technology of surfaces. D. Lichtman, who identified 56 separate techniques for measuring the composition of surfaces over a decade ago [14], indicates the number is now approximately 200 [15]. Various schemes have been used to organize conceptually the methods of compositional surface analysis, but perhaps the most logical approach is to consider the mode of surface excitation as input and the mode of detection as output [14]. Since this brief review paper is restricted to considering the most widely used techniques, the several diagrams used by D. Lichtman can be simplified to that shown in Figure 3-1. The input particle has a controlled energy, mass, and intensity; the appropriate mass or energy of the output particle is measured by the detector. Detectors may be concerned with the mass and charge of the particle, its energy, and spatial distribution. The interest, of course, is to correlate the detected information with the elements on the surface.

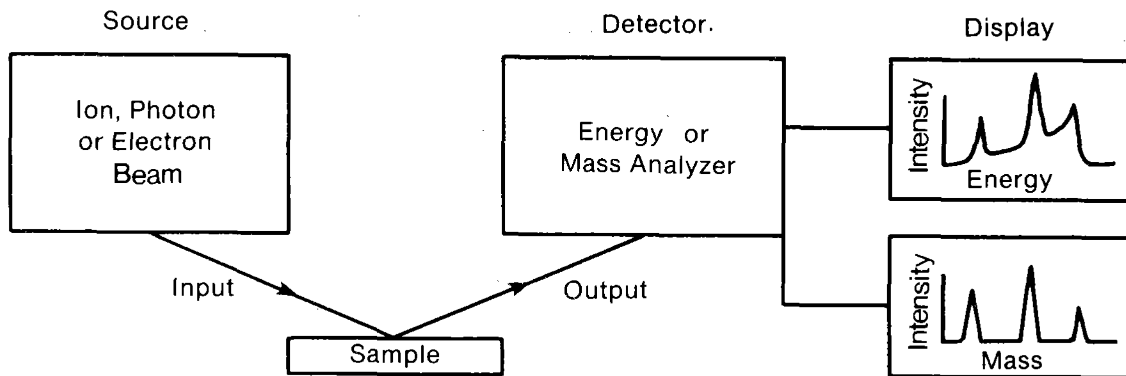

Figure 3-1. Generalized Input and Output Probes for Surface Analysis. The Electron Energy (AES, XPS), Ion Energy (ISS, RBS), and Ion Mass (SIMS) Are the Measured Output Parameters.

3.1 SECONDARY ION MASS SPECTROMETRY (SIMS)

In SIMS, a beam of primary ions is directed towards the sample surface, where most of the energy of the ions is dissipated into the near surface region of the solid by a series of collisions. As a result of the increase in energy of the solid and of the multiple collisions, surface and near-surface atoms are ejected (sputtered) from the solid (Figure 2-3). Some of the particles are sputtered as secondary ions, and these are accelerated into a mass spectrometer for analysis. Although early SIMS experiments were carried out in the late 1930s and the feasibility of SIMS was clearly demonstrated by R. Herzog and R. Viehböck in 1949 [16], the activity did not widen until the late 1950s as a result of R. Honig's work [17]. A large number of excellent reviews concerned with secondary ion emission and the applications of SIMS to surface and thin film analysis have been documented in reviews by J. McHugh [7], H. Werner [10], A. Benninghoven [18], and G. Blaise [19] as well as by those who provide emphasis on aspects related to SIMS [6,8,9,11,12,20].

3.1.1 Physical Principles and Processes

The detected signal of the ith element in SIMS requires controlled destruction of the surface and subsurface of the sample to produce a secondary ion current $I_i^{\pm}$. The current for the ith element depends on many factors that may be related by the expression

$$I_i^{\pm} = I_p f_i^{\pm} C_i S_i \eta_i \ , \qquad (3\text{-}1)$$

where I_p is the incident ion current (ions/s), S_i is the sputtering yield of both ions and neutrals (particles/incident ion), $f_i^{\pm}$ is the fraction of the particles sputtered as ions, C_i is the concentration of the ith element (corrected for isotopic abundance) in the sputtered volume, η_i is the collection efficiency of the SIMS instrument, and ± refers to a positive or a negative particle.

A basic understanding of the surface analysis capabilities of SIMS requires consideration of the interdependence of the incident ion beam current, beam diameter, current density, surface removal rate and detection sensitivity as plotted for typical situation in Figure 2-1 by J. McHugh [7]. For the situation described, removal of one atomic layer per hour will require 0.2 nA for a FWHM beam of 1 mm, providing a current density of ~50 nA/cm^2, and a detection sensitivity of about 50 ppm. This low removal rate also requires a vacuum of 10^{-6} Pa to prevent contamination, assuming the sticking coefficient is unity for the residual gases present. (Note: Many materials have sticking coefficients ranging from 0.1 to 0.001 for H_2 and CO, a point often ignored in the literature when vacuum requirements are discussed.)

Most SIMS instruments can be operated in a mode to detect either positive or negative ions, so I_i^+ or I_i^- can be considered separately in Eq. 3-1. Since C_i depends on the sample selected, consideration will now be given to S_i, I_p, and f_i.

The factors affecting the sputtering yield during ion bombardment are given in Section 2.1. The most important parameters influencing the sputtering yield are the energy, mass, and incidence angle of the projectile ion. Typical

bombardment energies range from 1 to 20 keV with argon the most frequently used gas. For example, the sputtering yield increases steadily up to about 50 keV for $Ar^+ \rightarrow Cu$, and a threefold increase in S occurs between 1 and 10 keV. The combined effects of mass, energy, and angle for sputtering copper with Xe^+ at 110 keV and 60° from the normal provides a sputtering yield that is about 250 times greater than when using 1 keV He^+ at normal incidence!

For the fraction of secondary ions produced $f_i^{\pm}$ efforts to date indicate that resonance and autoionization of excited species leaving the solid are the major sources of the secondary ion fraction [7]. Resonance ionization of ground state sputtered neutrals is considered to make a less important contribution.

The following facts have been determined experimentally. Most sputtered particles leave the surface with energies of only a few eV. The secondary ion yields from nonconducting metal compounds are typically 10^2 to 10^3 times the yields from the corresponding metals [18]. The mean velocity of sputtered particles is greater for materials with high binding energies (insulators versus metals), and the higher velocity components of the distribution of sputtered particles are ionized with greater efficiency.

The secondary ion species are mainly singly charged atomic and molecular ions (mainly dimers). Doubly charged atomic species and trimers are also formed and these, combined with the high sensitivity of mass spectrometers, play an important role in producing complex spectra. Furthermore, the presence of anions (example, oxides) results in the formation of M_xO_y, where x and y are integers [18].

The current density and chemical nature of the primary ion also have a marked influence on I^+ or I^-. Since I_p (ions/s) = $0.25\ \pi d^2 j$, where d is the diameter (FWHM) of the Gaussian-shaped beam and j is the current density (ions/cm^2 s), it is seen I^+ or I^- is directly proportional to the number of ions incident on the target. The proportionality remains valid even for current densities as large as $10^5\ \mu A/cm^2$. A potential problem at high current densities is an increase in the sample temperature.

The most important influence of a primary ion is its chemical identity, especially when reactive gases are used. For example, Figure 3-2 shown in J. McHugh [7], shows an increase in the secondary ion yield for an iron surface when the primary beam is either oxygen 16 or argon 40. An increase in the Fe 56 peak after 40 s is attributed to the enhancement of the sputtering yield by using oxygen, which continuously changes the composition as new subsurface atomic layers are exposed. Many examples may be found where reactive gases, particularly oxygen and nitrogen, have been used to increase the secondary ion current.

3.1.2 Experimental

All SIMS instruments require a vacuum chamber, a primary ion source for bombardment, a mass spectrometer for mass analysis of the sputtered ions, a sample holder, and means for displaying and processing the spectra, as shown in Figure 3-2. Summaries and comparisons of various commercial instruments,

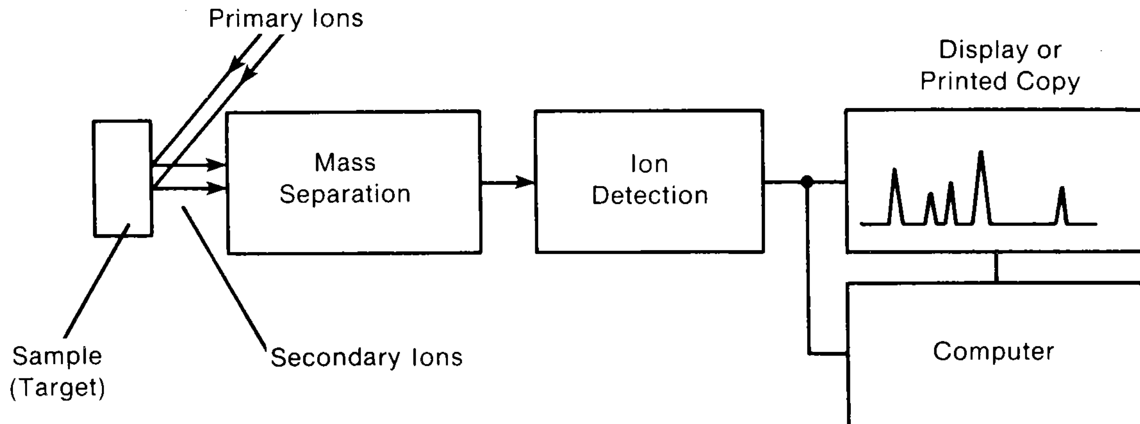

Figure 3-2. Principle of SIMS (see Ref. 10).

their designs, and cost have been made by C. Evans [21] as well as by J. McHugh [7] and H. Werner [10].

The instruments have been categorized as secondary ion mass analyzers (SIMA) and ion microprobes. The latter provide imaging capabilities. In conventional SIMA, the ion optics are arranged to focus all secondary ions at a point in front of the detector, which precludes the possibility of imaging. Distinctions between ion microprobes are sometimes made on the basis of the different methods used to obtain an image of the sample. Ion microprobes cost 3 to 10 times that for SIMA.

Most instruments have vacuum capabilities in the very high vacuum region ($\sim10^{-5}$ to 10^{-6} Pa) rather than UHV, primarily because the high sputtering rates used for depth profiling erode the sample surfaces faster than they can be contaminated by the residual gases present. In more recent versions of SIMA, a quadrupole mass filter is used as the mass analyzer and UHV capabilities range from 10^{-10} to 10^{-11} Pa. As indicated earlier, if slow sputtering rates are used for analysis of the first one or two monolayers; e.g., with a beam size 1 to 10 mm^2, the vacuum capabilities must be improved to prevent recontamination from the residual gases. An additional factor here is that surfaces damaged by bombardment are usually more reactive than undamaged surfaces.

The secondary ions may be mass analyzed using a quadrupole mass filter or a conventional mass spectrometer. Most SIMA use a single focusing mass spectrometer or a quadrupole mass filter, whereas the ion microprobes typically use a double focusing mass spectrometer. The advantages and disadvantages of the various schemes used to detect the secondary ion current have been treated

in-depth in various review articles [7,10,21]. The outstanding difference is a 500-1000-fold improvement in the lateral resolution in the ion microprobes--at the cost of 3 to 10 times that of SIMA with a single focusing mass spectrometer or a quadrupole.

Secondary positive ion yield intensities for elements present on a silver standard are shown in Figure 3-3 for a SIMA with a Balzers quadrupole mass spectrometer. The spectrum is complex, as expected. The mass spectra of negative sputtered ions also contain a large number of components corresponding to the many different negatively charged clusters that are ejected.

Hundreds of SIMS spectra have been published. The reader is referred to the review articles [7,10,11,12,18,19,20] that have many excellent examples of specific applications and that contain numerous additional references to the literature. The main features of the spectra are precise identification of the masses of secondary ions sputtered from the surface and near surface of the sample. The resolution of the masses is as good as the mass filter or spectrometer employed, usually unit resolution to amu 300 as a minimum. In contrast with other surface techniques, the complex spectra provide a great deal of information about the intensity of sputtered complexes, which makes the interpretation of the data much more difficult.

3.1.3 Advantages and Limitations of SIMS

In addition to the ability to provide identification of elements on the surface of conductors, semiconductors, and insulators, there are many other advantages for using SIMS. These include the ability to detect H and He on the surface, which is physically impossible with AES and XPS and is only possible with ISS using ^{3}He for the probe ion and scattering angles below 19.5^o for protons and below 41.8^o for deuterons.

The outstanding feature of SIMS is a detection sensitivity of about 10^{-6} to 10^{-4} of a monolayer for surface analysis, depending on how fast the surface is sputtered away. Except for slight variations in the transmissivity of ions with different masses, there is no Z dependence on the detection sensitivity of a properly designed SIMS apparatus. Furthermore, the absence of an inherent background permits detection of trace amounts of 10^{-2} to 1 ppm atomic. As little as 10^{-18} g of a sample species may be sufficient to provide a detectable signal, Thus, using care in the instrument and bombardment parameters, signals can be restricted to 1-2 monolayers.

The sensitivity of SIMS to different isotopic masses provides new possibilities for studying corrosion mechanisms, self-diffusion phenomena, and surface reactions involving any exchange of atomic species. Isotopic labeling of both cations and anions could be used for studying reaction mechanisms. Despite the apparent potential, the literature contains little mention of isotopic labeling with SIMS analysis of the surface.

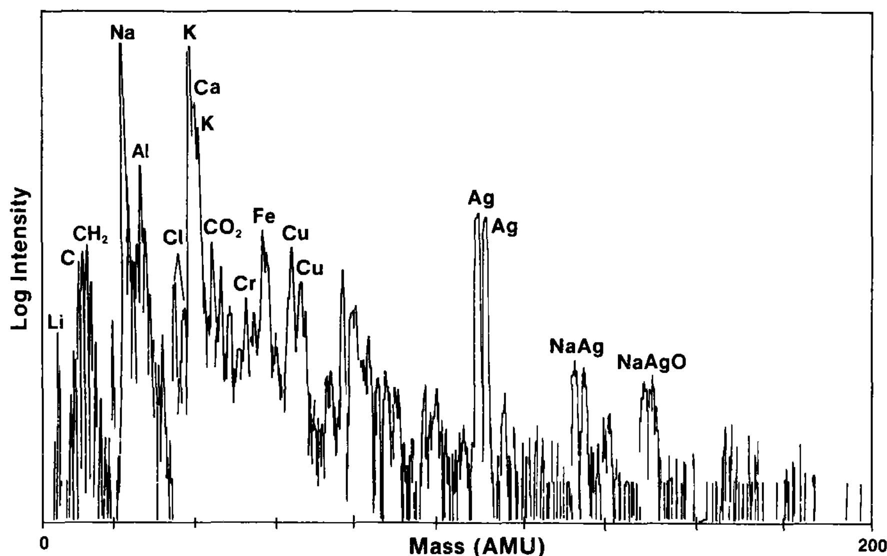

Figure 3-3. SIMS Spectrum of a Silver Standard.

Although mentioned in the introductory paragraph, the detectability of hydrogen by SIMS provides a routinely available capability not possible with other commercially available surface analysis equipment. In addition to the widespread interest in hydrogen interaction with potential materials for the first wall of magnetic fusion reactors, there is a general interest in the contamination of sputtered surfaces with the residual gases in UHV environments (mostly H_2 at $P < 10^{-7}$ Pa).

The complex spectra presented also provide an opportunity to unravel chemical information about surface compounds. The present work here is in the early stages of development, but the various fractions of M_xO_y and their clusters (for oxide surfaces as an example) should be related to statistical processes for destruction of the surface bonds.

The ability to depth-profile and to maintain a constant monitor of the composition is one of the outstanding features of a SIMS apparatus. The obvious application here is to detect, down to the 10^{-6} to 10^{-8} level, impurity accumulations at solid-solid interfaces lying hundreds of atomic layers below the outer surface. As with any depth profiling process, the resolution at the interface is limited by the damage from sputtering rather than by the apparatus.

Ion microprobes provide capability to image the surface under investigation. This, combined with outstanding lateral resolution, provides a capability for analyzing the composition of individual grains in polycrystalline materials and for determining the distribution of elements (bulk or trace) across the surface. For example, an average surface concentration of an undesirable

component of 10^{-3} monolayers may be far worse if it is distributed as small particles over a surface rather than as a few large clusters.

For limitations, SIMS requires destruction of the sample for analysis; there is no chance for a second look at the same spot on the sample. The factors causing large variations in the production of secondary ions make routine quantifications a remote hope unless standards are used in well studied systems. Finally, matrix effects; e.g., the variation in the signal of the same element in different chemical environments, can alter the detectability of trace amounts by factors of 100 to 10,000.

3.2 ION SCATTERING SPECTROMETRY (ISS)

In ISS, a collimated monoenergetic beam of ions of known mass (M_1) is directed towards a solid surface and the energy of the ions scattered from the surface is measured at a particular angle. The energy E_o of the projectile ion is reduced to E during a collision with a surface atom (M_2) and the intensity of scattered ions is measured and normally presented vs. E/E_o in an energy loss spectrum. From the number of scattered ions of mass M_1 appearing at particular E/E_o ratios, information may be deduced about the mass and number density of the various surface species in the target; i.e., the elemental composition of the surface. Since D. Smith [22] first demonstrated the feasibility of ISS as an analytical tool, a number of review articles have been written by other early users of ISS [14,23-29]. The important elucidation of Smith is that important aspects of the energy loss spectrum can be explained by considering the ion-surface atom collision as a simple two-body event.

3.2.1 Physical Principles and Scattered Ion Yield

An ion scattered from a surface atom is shown schematically in Figure 3-4. Using the single binary elastic collision model; i.e., ignoring all interactions with other atoms and applying conservation energy and momentum, the energy E of the scattered ions of mass M_1 with an incident energy E_o scattered at a laboratory angle θ is

$$E = E_o(1+\alpha)^{-2}[\cos\theta + (\alpha^2 - \sin^2\theta)^{1/2}]^2 , \qquad (3\text{-}2)$$

provided that $\geqslant 1$, where α is M_2/M_1. The energy after the collision depends on E_o, M_1, M_2, and θ. It is customary to represent the experimental data as scattered ion current vs. E/E_o and to fix θ and M_1 during the experiment so peaks in the energy loss spectrum E/E_o correspond to M_2 values deduced from Eq. 3-2.

For Eq. 3-2, it was assumed the binary collision model is valid. It was also assumed that the target atoms are stationary and are not coupled to their neighbors because typical lattice vibration times of about 10^{-13} sec are large compared with a collision time of 10^{-15} to 10^{-16} sec and the thermal energy/atom at 25°C is only about 0.04 eV compared with typical incident ion energies of 0.5-3 keV. For the energies used, the de Broglie wavelengths are small compared with atomic dimensions, so classical mechanics provides an adequate description of the collisions.

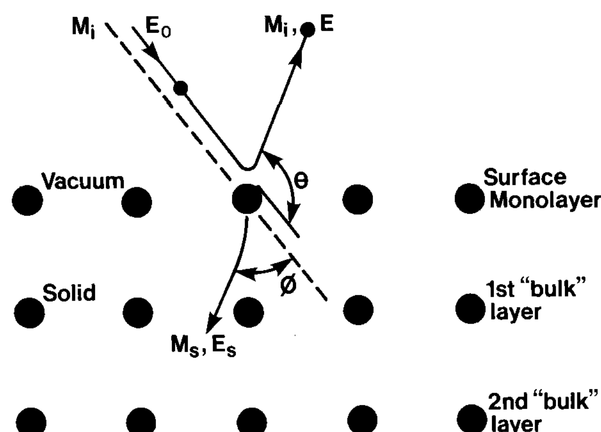

Figure 3-4. Schematic Representation of the Scattering of a Projectile Ion from a Surface Atom and the Recoil of the Surface Atom M_2 with the Energy E_2.

The signal intensity I_i^+ resulting from the scattering of an ion beam by surface species M_i can be expressed by

$$I_i^+ = I_o(N_i - \beta_j N_j)P_i(d\sigma(\theta)/d\Omega)_{\theta_{SC}}\Delta\Omega \tag{3-3}$$

where I_i^+ is the signal intensity originating from a surface species M_i, I_o is the primary beam intensity, N_i is the number of scattering centers (mass M_i) per unit area, β_j is the shadowing factor for the species M_i due to the coverage of another surface species of density N_j, P_i is the probability that an incident ion will not be neutralized, $(d\sigma_i/d\Omega)_{SC}$ is the differential scattering cross section evaluated at the scattering angle θ_{SC}, and $\Delta\Omega$ is the solid angle seen by the detecting system. In Eq. 3-3, I_o and $\Delta\Omega$ are determined by the instrumental parameters chosen. The solid itself affects N_i, $d\sigma_i/d\Omega$, and P_i. It can be presumed the signal intensity is directly related to N_i.

For a pure substance with no adsorbed species ($N_j = 0$), the exposed surface atom density depends on the crystal plane exposed. In general, β_i can be related to all geometric considerations that affect the visibility of the target atom to the probe ion. The Z dependence of $d\sigma/d\Omega$ typically increases by a factor of ten from low to high Z. If a reasonable interaction potential is known or can be assumed, the differential scattering cross section can be derived using the methods of classical mechanics. The screened Coulomb potential, $V(r) = Z_1Z_2e^2r^{-1}$ exp $(-r/a)$ has been used most frequently by ISS users. Tables have been published from which differential scattering cross sections can be derived [30,31]. The essential point is that the signal

intensity is not strongly dependent on different forms of interaction potentials. As described in the next section, cross sections for multiple and subsurface collisions can be ignored because of neutralization processes.

Perhaps the most important, and least understood, parameter in Eq. 3-3 is the probability that an incident ion will not be neutralized. Depending on the energy, only about 0.01-10% of the projectile ions are scattered as ions; the remaining ions experiencing binary collisions are neutralized. The projectile ion approaches the surface with a deep potential well available for an electron (-24.4 eV for He^+, -21.6 eV, for Ne^+ and -15.5 eV for Ar^+) compared with a work function of about 5 eV for a typical solid. Since the closest approach during a large angle collision encounter is of the order of 0.01 nm, the quantum mechanical probability that electrons will tunnel from the solid to the ion is high. The details of the neutralization process during the approach, collision encounter or flight from the surface have not yet been established. Energetically feasible models, recently considered by C. Moyer and K. Orvek [32], include resonance and Auger neutralization [27]. The more vigorous approach to the quantum mechanics of the incident ion shows that resonance neutralization is much more important than previously thought and indeed may be the dominant process.

Oscillations in I^+ for helium scattering from Pb, Bi, In, Ga, Ge, As, Sn, and Sb have been summarized [33]. The detailed shapes of the oscillatory curves for these elements have been shown to depend on their chemical environment [34]. The oscillations in I^+ result from quasi-resonant electron charge transfer between the surface atom and the incident ion, similar to that observed for scattering between ions and gas-phase atoms. The entire subject of neutralization of projectile ions by a solid surface deserves careful further study.

3.2.2 Experimental

Although the facilities needed vary with the goals for a particular problem, the essential needs for ion scattering experiments are a vacuum chamber, an ion gun, a target, and an energy analyzing system.

Ions are produced in a source by electron bombardment of a gas, usually He, Ne, or Ar. With the source held at the desired accelerating potential (~0.3 to 3 keV), ions are drawn from it by a negatively biased electrode. An ion beam is formed by an ion focusing lens system. For most applications, only one type of singly charged ion species is desired in the beam; e.g., ^3He, ^4He, ^{20}Ne, or ^{40}Ar.

Important properties of the ion gun include producing a beam with an energy spread of only a few eV, a current in the range of 1 to 300 nA, and an angular divergence not greater than ±1°. The beam typically has a Gaussian shape in the ion number density with a FWHM ranging from 0.1 to 3 mm, depending on the focusing voltages. The beam current must be stable so that repetitive scans of E/E_o from 0 to 1 will be responding to the same integrated projectile ion flux in ions/cm^2. Velocity filters, mass separators, differentially pumped sources, and gas exchange are techniques used to maintain probe gas purity.

The vacuum chamber must provide base pressure and residual gas background capabilities compatible with the samples to be investigated. Thus, the base pressure may range from 10^{-5} to 10^{-8} Pa for a UHV system of stainless steel construction. The sample holder serves as a conducting path for measuring the ion beam current in addition to its obvious use. Any material that is vacuum worthy can serve as a suitable sample.

Scattered ions are detected by using an energy analyzer either of the sector cylindrical mirror or hemispherical type and an electron multiplier detector. For most instruments, θ is fixed, but in custom made spectrometers it may be varied.

An ISS spectrum, which is obtained by simultaneously ramping the analyzer plate voltage and recording the output signal, consists of a series of peaks in the scattered ion current. The peaks occur at values of E/E_0 determined from Eq. 3-2 by substituting for M_2 the masses of the surface atoms. In practice, the peak locations in E/E_0 are precomputed for all elements so that identifying surface species is simply reduced to reading a table that lists the chemical elements vs. E/E_0 for each noble gas probe ion.

Typical spectra for 1500 eV ^{3}He incident on polypropylene and on isotopically labeled copper oxide on various substrates are shown in Figure 3-5 [35]. The peak positions correspond to C, ^{16}O, ^{18}O, Na, Pt, Cu, and Au, respectively. In Figure 3-5b-d, ion etching of the copper oxide was carried out until the oxide-substrate interface was reached as evidenced by the small signal intensity from Na, Pt, or Au.

The main feature of ISS spectra is that only one peak appears for each element, or isotope of each element, as predicted from the theory outlined in Section 3.2.1. Thus, six elements will yield only six peaks, a situation that is considerably simpler than other surface spectroscopies. While an ISS spectrum is simple, the peaks are broad and resolution between neighboring elements in the periodic table is poor, especially for high Z elements.

A considerable amount of additional information is available in ISS spectra, as summarized by W. Baun [36]. The yield curve of a typical ISS energy loss spectrum also contains low energy (sputtering) peaks, multiple scattering peaks, peaks from doubly ionized particles, and tailing on the low energy side of a peak from an elastic collision. W. Baun concludes that many scattered ion yield curves are rich in fine features that may be used to distinguish between elements with unresolvable ISS peaks or to obtain chemical information.

3.2.3 Major Advantages and Limitations of ISS

There are several major advantages for using ISS as a surface sensitive technique in addition to the obvious ability to identify elemental masses on solid surfaces for samples that are conductors, semiconductors, and insulators. Qualitatively, the current detection sensitivity is 0.01 to 0.001 monolayers

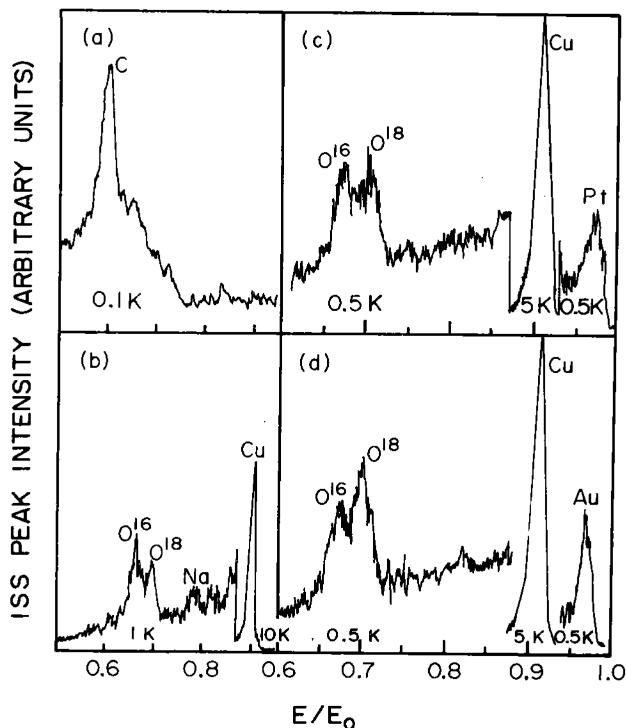

Figure 3-5. ISS Spectra for (a) Polypropylene, (b) $Cu^{18}O_{0.67}$ Film at the Oxide/Glass Interface, (c) $Cu^{18}O_{0.67}$ Film at the Oxide/Pt Interface, and (d) $Cu^{18}O_{0.67}$ Film at the Oxide/Au Interface (see Ref. 91).

for the light elements and 0.0001 to 0.00001 monolayers for heavier elements. Depth profiling is routinely accomplished by using the same ion gun for etching and supplying the projectile ions for scattering.

Monolayer sensitivity is the strongest advantage of ISS because the detected signal results primarily, and possibly only, from atoms in the outer monolayer. Ions that penetrate into the second or deeper layers have such a high probability of being neutralized that the ion yield from the second layers and lower is below detection limits.

Structural information can be deduced about the arrangement of two or more elements on single crystalline substrates. The location of S on Ni(100) and on Si(111) and of O on Ag(110), Ni(100), Ni(110), W, and Pb are among the recent examples cited [25,27] in which shadowing of the projectile ion beam was used. Structural information can also be deduced from using multiple scattering, particularly double scattering.

Isotopes of the same element can be detected, as reported recently for ^{16}O and ^{18}O in copper oxide films (Figure 3-5). The sensitivity of ISS to different isotopic masses provides a significant new dimension for ISS studies of catalytic reaction mechanisms, corrosion mechanisms, self-diffusion processes, adsorption-desorption phenomena or any surface reaction where there is exchange of the same atomic species. Furthermore, quantitative analysis for a particular species in a well-characterized system can be made from analysis of the peak height intensity [35] as expected from Eq. 3-3 where I^+ is $\propto N_i$ and

when all other factors are constant. Chemical information can be deduced about the influence of different chemical environments on the detected signal for the elements engaging in quasiresonant transfer processes [33].

The strongest limitation is that the resolution decreases as $M_1 << M_2$ and is reduced further because of broad peaks. Finally, the surface under investigation will be damaged by the bombardment from the projectile ions. Even though reduced bombardment energies (~300-700 eV) and low current densitites (0.4 to 40 $\mu A/cm^2$) may be employed, sputtering of the outer monolayer is unavoidable.

3.3 RUTHERFORD BACKSCATTERING SPECTROMETRY (RBS)

In RBS, a collimated monoenergetic beam of ions of known mass M_1 is directed towards a solid material and the energy of the ions scattered is measured at a particular angle. The initial energy E_0 of the projectile ion is reduced to E during the passage through the solid and by the collision with a surface or bulk atom. The intensity of scattered ions is measured and presented in an energy loss spectrum. From the intensity of scattered ions of mass M_1 appearing over ranges of E/E_0, information may be deduced about the number density, mass, and depth distribution of atoms at the surface or in the bulk. The conceptual foundations for RBS were built following the discoveries by E. Rutherford [37] and H. Geiger and E. Marsden [38] about the nuclear structure of the atom and the use of alpha particles to prove the model. Particle accelerators in the 1 to 3 MeV range became readily available in the late 1940s, and in the 1950s, RBS instruments were applied to analyze bulk composition [39]. Thin film and surface analysis with RBS, which was demonstrated in the late 1950s and early 1960s, respectively, have grown dramatically in the last decade as evidenced by an entire book being devoted to the subject in 1978 [40]. This book by W. Chu, J. Mayer, and M-A. Nicolet has a comprehensive bibliography of review articles, books on related material, and categorized applications.

3.3.1 Physical Principles

Ion scattering from surface and bulk atoms from a solid is shown schematically in Figure 3-6, but for RBS the incident energies are typically 1 to 3 MeV, rather than 0.5 to 3 keV as in ISS. The energy of scattered ions is reduced during the elastic collision by the amount given in Eq. 3-2; there are no nuclear reactions. However, the scattering cross section is greatly reduced at MeV energies, so backscattered particles reach the detector from hundreds of nanometers into the solid. As the ion travels through the dense solid, it loses an average energy, primarily by collisions with electrons around each nucleus, leading to the concept of a stopping cross section. Since the collision encounters are quantum, a monoenergetic incident ion energy will emerge from the solid with an energy distribution about its initial energy as a result of statistical fluctuations, which is termed energy straggling [40]. The energy of a backscattered ion then is reduced by the stopping cross section before and after the binary collision, so the mean energy of the ion provides a measure of the depth at which the collision occurred, as illustrated in Figure 3-6.

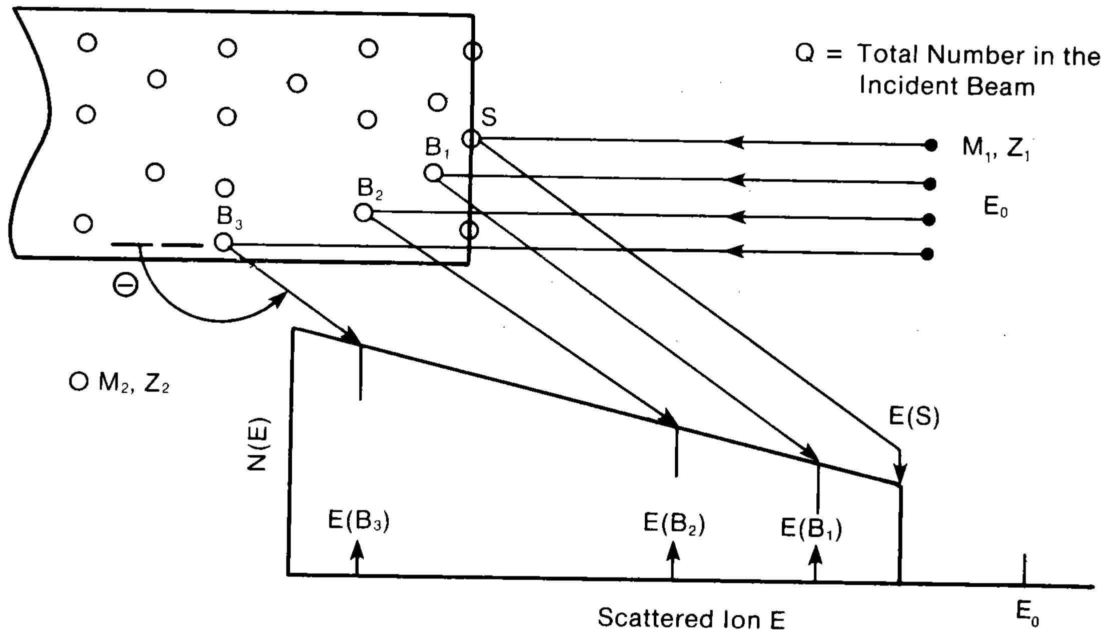

Figure 3-6. Schematic Representation of the Scattering of Projectile Ions from Surface and Bulk Atoms of M_2 and Z_2 Through a Scattering Angle θ to Form an RBS Spectrum (see Ref. 40).

The probability that an ion is scattered into a particular solid angle Ω is given by the differential scattering cross section dσ/dΩ. For small solid angles, the average differential cross section σ is approximately equal to dσ/dΩ, and is usually called the scattering cross section in the literature. The total number of detected particles Q_D resulting from MeV ion scattering into a solid angle Ω can be expressed by

$$Q_D = Q_o(Nt)\sigma\Omega \qquad (3\text{-}4)$$

where Q_o is the total number of incident particles, and Nt is the number of particles per unit area in the target. The principal difference between Eq. 3-4 and Eq. 3-3 is the absence of a neutralization probability. Both alpha particles and protons do not undergo charge exchange with a solid until their energy is somewhat less than 1 MeV. Notice also that Q_D is for all particles detected irrespective of their energy, which suggests multichannel techniques will be employed experimentally. Most significantly for RBS, the central force field is well-known, which means an expression for σ(θ) can be derived; calculations of σ(θ) for various values of M_1/M_2 are made by simply using an appropriate transformation of coordinates for treating a two body rather than a one-body problem. About 1 in 10,000 ions will be backscattered and very few of those will have scattering angles near 170°.

3.3.2 Experimental

The essential needs for RBS are a particle accelerator (usually 1 to 3 MeV), a solid state detector, and multichannel analyzer aside from the obvious need

for vacuum and a target. The important properties of particle accelerators; e.g., Van de Graaff generators, are well-documented [40]. Since the analysis is based on the reduced energy of a scattered particle, it is clear the initial energy should be accurately defined. The energy width at E_o should also be small because of energy straggling. The beam is typically passed through a quadrupole focusing magnet and magnetic analyzer prior to being incident on the sample at 10 to 100 nA and 1 mm^2. Most of the interest in RBS has centered on in-depth compositional analysis (without ion etching), so UHV requirements can be relaxed to high vacuum, unless surface sensitive information is sought.

Particles scattered into the solid angle are incident on the area defined by the aperture of the analyzing system, which has an analog output signal. This signal is processed by a multichannel analyzer, where each channel is an equal increment of the analyzer magnitude. An event whose magnitude falls into one of these several thousand channels is registered as a count. At the end of the experiment, a yield H_i for the ith channel; i.e., the counts registered by each channel, can then be displayed graphically. When an appropriate conversion is made for the energy range of particles detected by the ith channel, a backscattering spectrum may be displayed (solid line, Figure 3-7). The basic problem then is to relate the number of counts H_i to the scattering centers per unit area Nt_i in the layer thickness t_i at a depth X_i, which corresponds to an energy width ΔE and the position E_i of channel i in the energy spectrum. For a beam at normal incidence, we see that $H_i = Q_o N t_i \sigma(E_i)\Omega$, where $\sigma(E_i)$ is the cross section evaluated at E_i and averaged over the solid angle Ω. The sharp increase (KE_o, Figure 3-7) results from scattering from the surface of the film, where $K = E/E_o$. Spectra are shown in Figure 3-8 for a high Z homogeneous thin film on a low Z thick film and for a thin low Z film on a thick high Z material.

Extensive data are available for assisting in RBS data analysis as a result of nearly forty years of using accelerators in nuclear physics. These include the isotopes of materials and relative abundances, kinetic factors (E/E_o) for all atomic masses at various scattering angles for both helium 4 and hydrogen 1, stopping cross sections for the elements for various incident ion energies, scattering cross sections between helium and all Zs for various scattering angles, and the yield from the surface at various helium 4 scattering [40].

The main features of RBS spectra are illustrated in Figures 3-6 and 3-8. Only one peak appears for each element (or isotope) present, and the thickness of the element is directly related to the peak width. The peak height can be calculated from first principles, so RBS is quantitative. The data can be gathered in a matter of minutes, so the analysis is essentially nondestructive. The dynamics of changes, such as interdiffusion, can be studied in situ.

Additional valuable information can be obtained by using single crystals, a goniometer, and channeling (or blocking) techniques. The incident beam and a major crystallographic crystal axis are aligned and most ions are transmitted too deep into the solid to contribute effectively to a backscattered yield, except for those scattered from the surface. Epitaxial growth of a few monolayers of deposited material on a host single crystal is an example when channeling studies are extremely valuable [41].

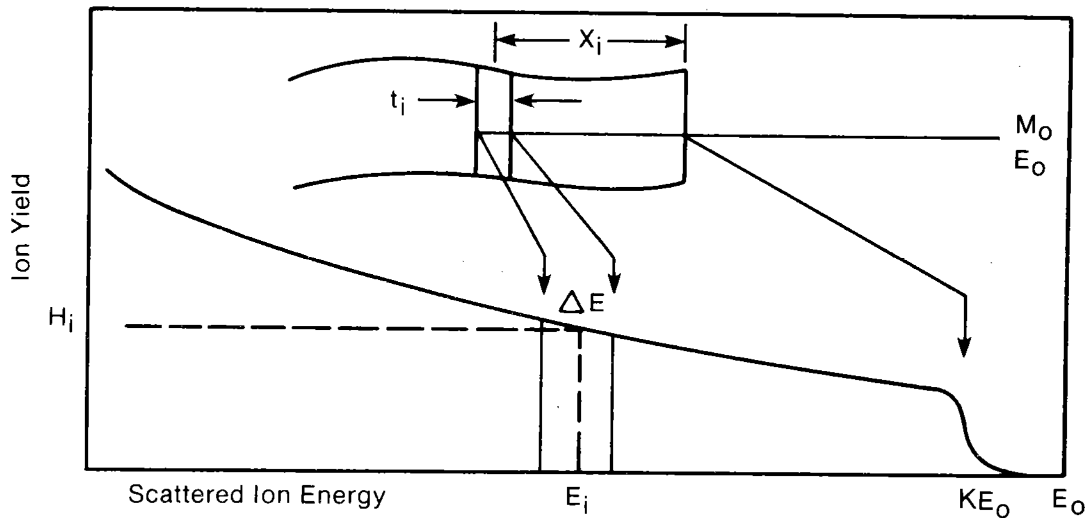

Figure 3-7. The Height H_i of the Ion Yield with Energies of ΔE from MeV Ion Scattering from Bulk Atoms of Thickness t_i at a Depth of X_i (see Ref. 40).

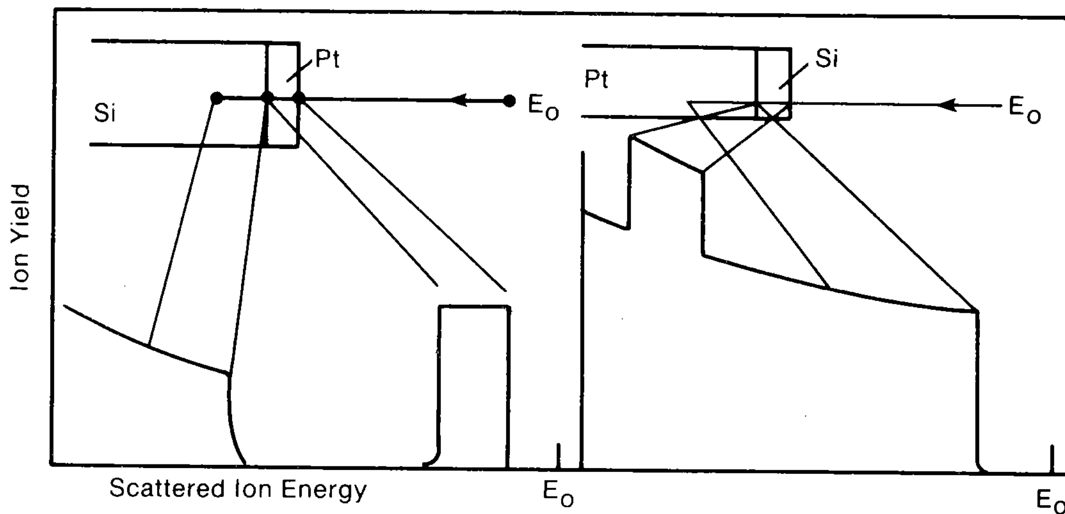

Figure 3-8. RBS Spectra for Scattering from a High Z Material on a Low Z

3.3.3 Advantages and Limitations of RBS

Quantitative and nondestructive in-depth compositional analysis are outstanding advantages of RBS. The quantitative capabilities result from the accurately known Rutherford scattering, cross sections, stopping cross sections, and the lack of ion neutralization at high energies. In-depth compositional detection is a direct result of small nuclear cross sections at high energies, permitting ion escape after a scattering event occurs deep within the solid without additional nuclear scattering.

The time to acquire data is only a few minutes, making it ideal for studying molecular dynamics within the same solid. The essentially nondestructive nature of RBS allows studying a single sample at such materials processing variables as temperature and time.

The technique is especially sensitive to high Z elements, so concentration levels down to 0.0001 atomic can be determined. At the same time, different isotopes of the same material are not resolvable, and the sensitivity for low Z elements is limited because their cross sections are about 100 times smaller than for high Z elements. Thus, sensitivities of 0.01 atomic are typically available for Be through F in the periodic table. Where isotopes are resolvable, there are similar advantages for RBS as stated for SIMS and ISS but at lower detection sensitivities for the low Z elements and lack of resolution for high Z elements.

The incident beam typically has a 1 mm-FWHM beam, so the lateral resolution is severely limited. Therefore, lateral sample uniformity is important; SEM sample analysis is also recommended to identify scratches, dust, and other defects. Furthermore, RBS as it is normally practiced is not surface sensitive, and the high vacuum chambers used precludes serious study of surfaces unless special vacuum chambers and single crystals are used. When single crystals or epitaxial layers are used, structural information, both at the surface and from the bulk, can be obtained by using channeling and blocking techniques. Finally, no chemical information can be extracted from the data.

3.4 X-RAY PHOTOELECTRON SPECTROSCOPY (XPS)

In XPS, an X-ray source is directed towards the solid surface and the energy of electrons ejected from the solid are measured with an energy analyzer. The ejected electrons have a kinetic energy equal to that of the incident photon energy minus the binding energy of the electron in the solid. K. Siegbahn and his co-workers first observed photoemission from solids in the 1950s, and the surface sensitivity of the process was published in 1966 [42]. Since then, a number of review articles [43-46] and books [47-50] have been written on XPS or electron spectroscopy for chemical analysis (ESCA), which is the acronym coined by the Swedish group [46].

3.4.1 Physical Principles

The basic XPS principle can be understood by referring to the electronic energy level diagram of Figure 3-9. An X-ray of energy $h\nu$ has the possibility

of ejecting any electron that has a binding energy (BE) of less than $h\nu$ with an intensity that is related to the photoelectric cross section. The zero[th] approximation is that every electron orbital level of energy ε will give rise to a peak in the XPS spectrum characterized by BE = ε. This is not strictly true, because on removing one electron from an n-electron system, the remaining n-1 electrons relax towards the hole created by the loss of the electron. Thus, BE < ε. In addition, it is this final state relaxation that is directly responsible for the probability of a two-electron process in which an electron is promoted from one of the valence level molecular orbitals to an unoccupied higher valence level simultaneously with the removal of the core electron, becoming greater than zero. This results in two or more peaks; i.e., a main peak and shake-up peak, appearing in the photoelectron spectrum for one ε value.

Another final state effect that gives rise to an increase in the number of photoemission peaks is multiplet splitting. If the valence levels contain unpaired electrons, as is often the case for transition metal materials, removal of a core-electron by XPS results in two possible final states with the spin of the remaining core-electron either up or down. The coupling with the unpaired spins of the valence levels will be different for up or down, and so the final state energies and hence the experimentally determined BEs will be different resulting in more than one peak in the photoemission process for a given initial state ε.

The essential principle is that every element in the periodic table has a unique set of electron binding energies, so qualitative elemental identification is assured from the measured kinetic energy; i.e., KE = $h\nu - \varepsilon$, as illustrated by Figure 3-10. The elemental peak intensities depend on the

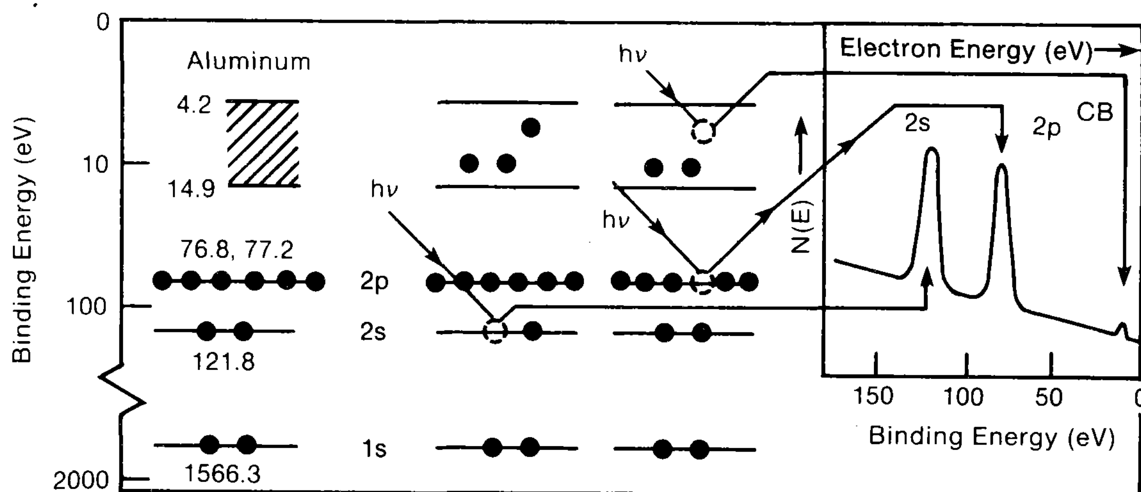

Figure 3-9. Electron Energy Levels for Aluminum Showing Ejection of 2s, 2p, or Valence Band Electrons by Photons to Produce the Intensity Shown in an XPS Spectrum of N(E) vs. Binding Energy.

photoionization cross section, as illustrated in Figure 3-11, and these are reasonably well-established [51,52]. The sensitivity of the lowest Z elements increases to Z = 12, where it drops dramatically. The repeated drops at higher Zs correspond to successive observations of 1s, 2p, 3d, and 4f electrons as those producing the strongest lines in XPS spectra. All elements which have core- levels; i.e., everything but hydrogen and helium can be detected, though the magnitude of the cross sections and hence the relative sensitivities to the different elements varies by $\sim 10^2$. Finally, quantitative analysis can be done reasonably well using methods described by C. Powell [53].

Electrons ejected from an energy level must escape from the solid without experiencing in elastic collisions and into the vacuum for detection. Since X-rays penetrate several hundred nanometers into the solid, it is essential to know the mean escape depth of the ejected electrons. A typical plot is drawn in Figure 3-12, which shows that a minimum mean escape depth of about 0.3 to 0.5 nm occurs at a KE of 100 eV. Thus, for a Mg X-ray source with $h\nu$ = 1254 eV, mean escape depths may range from 0.3 to about 3 nm. While this variation must be treated carefully for interpreting data, the escape depth information clearly establishes the sampling depth of identified elements.

The signal intensity I_i of the ejected electrons for the ith element is given by

$$I_i = F N_i \sigma_i \theta_i l_e TDG \tag{3-5}$$

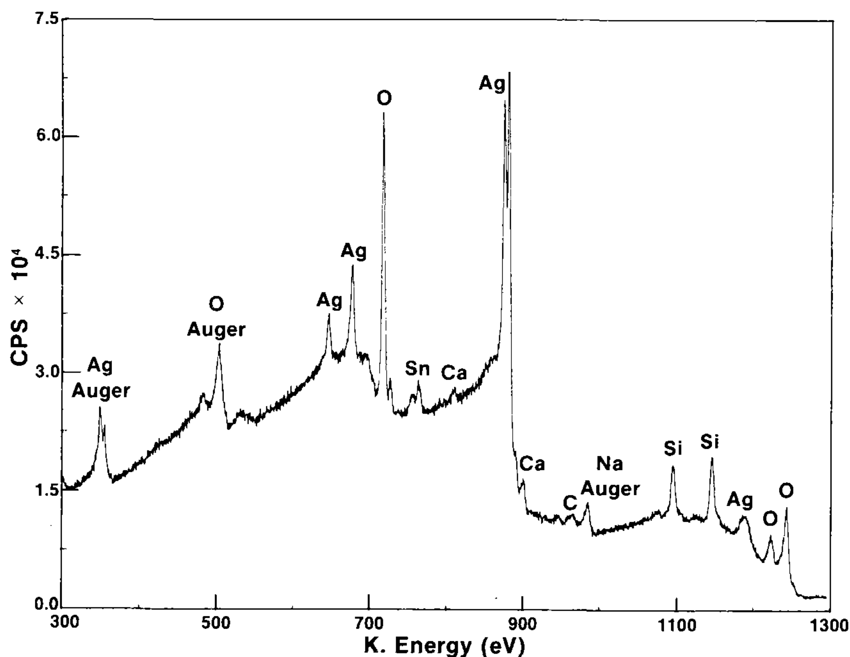

Figure 3-10. An XPS Survey Spectrum Showing the Presence of Ag, O, Sn, Ca, Na, Si, and C at the Silver-Glass Interface of a Mirror after Etching through 70 nm of Silver Deposited onto a Sensitized Glass Substrate (see Ref. 91).

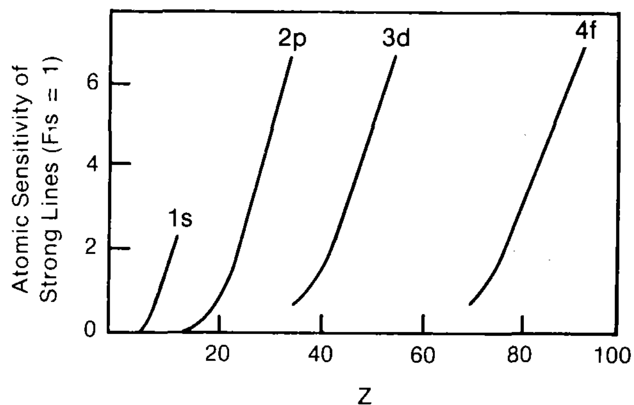

Figure 3-11. The Atomic Sensitivity of Strong Lines in XPS Spectra vs. the Atomic Number.

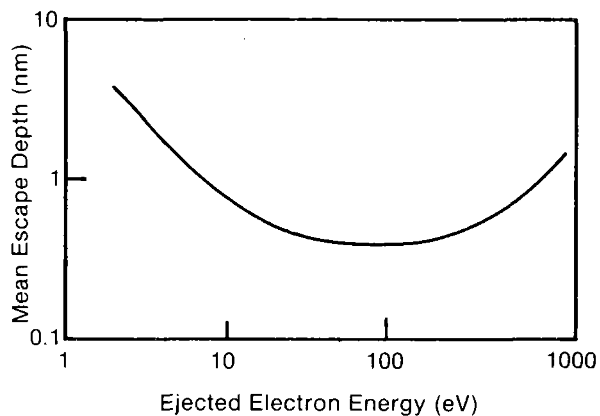

Figure 3-12. The Mean Escape Depth of Ejected Electrons vs. Energy (see Ref. 45).

where F is the incident photon flux, N_i is the atomic density, σ_i is the ionization cross section, θ_i is an asymmetry factor, l_e is the electron mean free path through the material, T is the analyzer transmission factor, D is the detector efficiency, and G is a geometric factor [53].

In addition to atomic identification, information on the chemical environment of the atom is available primarily from the chemical shift phenomenon. Small differences in BE (0-10 eV) occur with differences in the chemical environment of the atom. For metallic species, different oxidation states are usually distinguishable in this manner and for nonmetallic species, such as C, significant variations are observed depending on the electronegativities of the ligands [45]. Chemical shifts can be handled in some cases by theoretical means [50], but for most practical situations, a large empirical database is the preferred means of assigning shifts to particular chemical environments. The other two most common means of providing chemical information are from the shake-up and multiplet splitting phenomena. Since these effects are caused by electron transitions between occupied valence levels and since valence level energies are characteristic of the molecular or chemical state rather than the atomic state, the presence of structure due to shake-up and multiplet splitting provides additional fingerprinting of the chemical environment of an atom.

3.4.2 Experimental

The basic instrumentation for XPS measurements includes an X-ray source, a sample, an electron energy analyzer, a detector and recording system, and the vacuum chamber. The X-ray source is usually Mg or Al that yields energies of 1253.6 or 1486.6 eV, respectively. Synchrotron radiation sources provide a variable $h\nu$ and are especially good for producing electrons with the minimum escape depth. Energy analyzers are most commonly of the hemispherical/electrostatic type, except for the use of the cylindrical mirror type by one commercial instrument maker. Channel electron multipliers are also widely used for detectors. The energy resolution is limited to about 0.3 eV even by using monochromatic X-rays; the line width itself often exceeds 0.3 eV.

The sample itself should ideally be flat and about 1 cm^2 to provide maximum signal to the analyzer and detector. Even then, data accumulation for 20 to 30 minutes is required to secure a good XPS spectrum. The absolute sensitivity; i.e., the number of atoms required to give a detectable signal is not good by analytical standards. For typical instruments, 10^{13} to 10^{14} atoms are required. Since the sampling area is of the order of 0.5 cm^2, this corresponds to about 0.5 to 5% of a monolayer as the detection limit, if all the 10^{13} to 10^{14} atoms are in the top layer.

3.4.3 Advantages and Limitations of XPS

XPS is the most quantitative of the surface sensitive techniques, although in practical situations it is often limited by a combination of an unknown depth distribution over the probing depth. It quite obviously provides detection of all elements except hydrogen, all with reasonably well known cross sections and without strong matrix effects. It is especially sensitive for detecting low Z elements.

Excellent chemical information is obtained from shifts in the energy levels of the same atom in different oxidation states and chemical environments. Satellite structures with a well documented data base on standard compounds also are valuable for extracting chemical information.

XPS is the least destructive of the major techniques described in this section. This is because an X-ray source is used, and for related applications with synchrotron or UV sources, even less damage is introduced into the sample. Easily degradable materials, especially organic polymers, can be studied routinely with XPS but only selectively using ion or electron excitation sources.

As a surface technique, XPS is sensitive to 2 to 30 monolayers, depending on the material. However, by using special procedures; e.g., grazing exit XPS, a sensitivity to the top one or two monolayers is easily realizable.

For depth profiling, XPS has limited usefulness as a practical matter. This is because the long data accumulation times precludes simultaneously analyzing and ion etching. However, XPS has revealed that changes in the chemical state of some elements occurs during ion bombardment.

As the other principle limitation, XPS has the poorest lateral resolution of all the methods discussed. Photon sources are not easily confined to exciting small sample areas, and even when this becomes possible, the signal-to-noise problem may require even longer data accumulation times.

3.5 AUGER ELECTRON SPECTROSCOPY (AES)

In AES, an electron source is directed towards the solid surface to form vacancies in one of the core electron energy levels and the energy of electrons ejected from the solid are measured with an energy analyzer. The ejected Auger electrons have a kinetic energy approximately equal to that of the energy released from filling a core level minus the binding energy of the Auger electron prior to ejection. P. Auger discovered the effect named after him in 1925 [54], but it was J. Lander who suggested surface impurities could be identified by using electron stimulation of the solid [55]. The high sensitivity and broad applicability of the technique was not realized until L. Harris demonstrated the use of differentiation of the emitted electron energy distribution, N(E) vs. E, to obtain AES spectra in their current familiar form [56]. The rate of growth of AES from that time was absolutely phenomenal, because elemental identification was the crucial unknown precluding better understanding in surface science and technology and because of the low cost of modifying widely used, low energy electron diffraction (LEED) optics to perform LEED-AES studies. Numerous review papers [53,57-63] and, more recently, books [49,64] have been written detailing both the theoretical and experimental foundations of AES as well as scanning Auger microscopy (SAM).

3.5.1 Physical Principles

The Auger process can be understood by considering the ionization of an isolated atom under electron bombardment. The potential energy necessary to initiate an Auger electron transition is derived from the energy of a vacancy in an underlying core electron energy level. It is immaterial to the transition process how the vacancy came to exist. When a core level is ionized, the vacancy is immediately filled by another electron, as depicted by the $L_1 \rightarrow K$ transition in Figure 3-13. The energy ($E_K - E_{L_1}$) from this transition can be released as characteristic X-rays (basics for X-ray fluorescence spectroscopy) or be transferred to another electron; e.g., in the L_2 level, which is ejected from the atom as an Auger electron with a kinetic energy KE_A. The measured energy for an Auger deexcitation is given approximately by

$$KE_A = E_K - E_{L_1} - E_{L_2} - \phi_A , \qquad (3\text{-}6)$$

where ϕ_A is the work function of the analyzer material. This process is termed the KL_1L_2 Auger transition and clearly involves forming a K core vacancy by ionizing a 1s electron, filling the vacancy with a 2s electron in the L_1 level, and ejecting a 2p electron from the L_2 level. Auger transitions involving the KLL, LMM, and MNN levels are the most common although MMM, NNN, NNO, NOO, and OOO have also been identified and used. The binding energies for all electron energy levels have been plotted [47].

The Auger electron process clearly involves three electrons; one for forming the core vacancy, one that fills it, and the ejected Auger electron. The value of KE_A is determined by the differences in the energy levels for an atom of a particular Z. The core level electrons can be ejected from the solid by the primary electron and these also will have characteristic kinetic energies KE_c given by; e.g., $KE_c = E_p - E_K$, where E_p is the energy of the incident electron beam and E_K is the core electron ejected by the primary. By varying E_p, the values of KE_c will change whereas those of KE_A do not. These "characteristic loss electrons" are especially useful for assessing if sample charging is shifting the position of Auger electrons.

The intensity of a particular Auger electron emission; e.g., KL_1L_2, is proportional to the current of ionizing particles passing through the escape volume, the density in the volume, and the probability an ionizing event will occur in the K level; the latter is the cross section. The Auger current is reduced further by the acceptance angle and transmission of the analyzer as well as the Auger transition probability. An estimate of 0.32 nA was made for the Auger current incident on the detector from C on W for a primary beam current of 0.01 mA [63]. More rigorous considerations have been summarized by C. Powell [53], and the result is similar to Eq. 3-5.

Quantitative analysis with AES is not as simple as in XPS. First, the process is more complex, involving three electron levels instead of one. The core-level photoionization or electron impact cross section has to be folded with the Auger transition probability. The latter is not as well-known as photoionization cross sections, which makes quantitative analysis from first principles more difficult. Experimental standards are also less well-established. Finally, the usual manner of recording Auger spectra in the first derivative mode (dN(E)/dE) and measuring peak-to-peak heights can

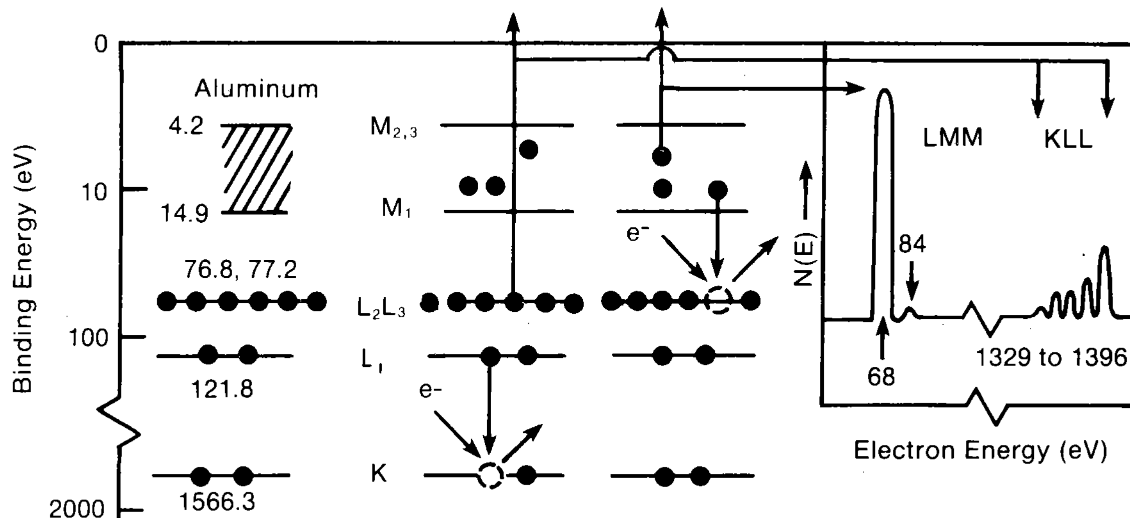

Figure 3-13. Electron Energy Levels for Aluminum Showing Ejection of a K or an L Electron by Incident Electrons to Produce the KLL or LMM Auger Electron Intensity in a Spectrum of N(E) vs. Electron Energy.

introduce large errors because of line shape changes; however, areas under AES peaks can now be integrated from output of N(E) vs. E.

All the chemical shift, shake-up, and multiplet splitting information of XPS is, in principle, available in AES. The interpretation is more complex, however, because of the three levels involved in the process. Auger chemical shifts have not been nearly so widely exploited as they have in XPS. The empirical database is currently much more limited, and again the habit of recording in the first derivative mode has obscured the usefulness of the chemical information. The exceptions are usually XPS researchers, who take their X-ray-induced Auger data in the same manner as the XPS data and treat the analysis in a similar manner.

It should be pointed out that the chemical shifts observed in AES are not usually the same as in XPS for the same atoms in the same chemical state. Often, they are larger because of the two-hole nature of the final state in the Auger process. The difference between the XPS and Auger chemical shift has been termed the Auger parameter [65] and is an additional useful guide to the chemical state of the atom concerned.

3.5.2 Experimental

The basic instrumentation for AES measurements includes an electron beam source, a sample, an electron energy analyzer, a detector, a recording system,

and a vacuum chamber. The electron beam source will usually have a series of selectable fixed primary energies in the range up to 10 keV; energies of 2, 3, 5, and 10 keV have been widely used. The primary source of electrons may include deflection plates to raster a finely focused beam over a sample area. In recent years, minimum beam sizes have been decreased from nominal 5000 to 200 to 50 nm FWHM's, providing exceptional lateral resolution and increased current densities that require special experimental caution.

Energy analyzers have been (in the order of progressively greater use) of the retarding grid, cylindrical mirror, and hemispherical types. Most commercially available instruments now use hemispherical analyzers, so the entire analyzer detection system for XPS and AES is identical. The smaller beam sizes place less stringent requirements on the sample size and topographical conditions for the analysis. However, the widespread coupling of AES and SAM with ion etching places initial demands on the initial flatness for securing better profiles.

3.5.3 Advantages and Limitations of AES

Auger spectroscopy, which is probably the most widely used method of surface compositional analysis, has a number of outstanding advantages. It is the fastest of the common methods for identifying elemental composition, and that feature combined with superb lateral resolution has even made it possible to obtain SAM maps of several elements during depth profiling. AES is especially good for depth profiling at high ion etching rates again because of its speed for data acquisition. A typical AES spectrum run and profile is shown in Figure 3-14. AES is sensitive to 2-10 monolayers, but unlike XPS, there is no way of changing the escape depth of the detected electrons, except for the loss electrons. It is also more sensitive to the light elements.

Most data have been collected in the dN(E)/dE vs. E mode for practical reasons as shown in Figure 3-14. However, with an increasing number of studies now securing N(E) vs. E AES data, an increasing amount of chemical information should be extracted from the experimental work. The chemical information appears as different shapes of particular peaks, and this has been largely obscured in the past.

Principal limitations in AES include damage to the sample by the electron beam, including introducing artifacts known as electron stimulated desorption. Severe charging problems may also develop, especially with poorly conducting materials. Negative charge must be supplied to all samples during analysis because of the net ejection of electrons from the sample by Auger processes. There is no sensitivity to atomic masses, so many of the mechanistic processes involving atom transport or exchange cannot be elucidated by isotopic labeling. Finally, there are many possible Auger processes that may occur, especially for the high Z elements. Even for analyzing binary alloys, peak interference problems may be encountered that complicate the interpretation of the data.

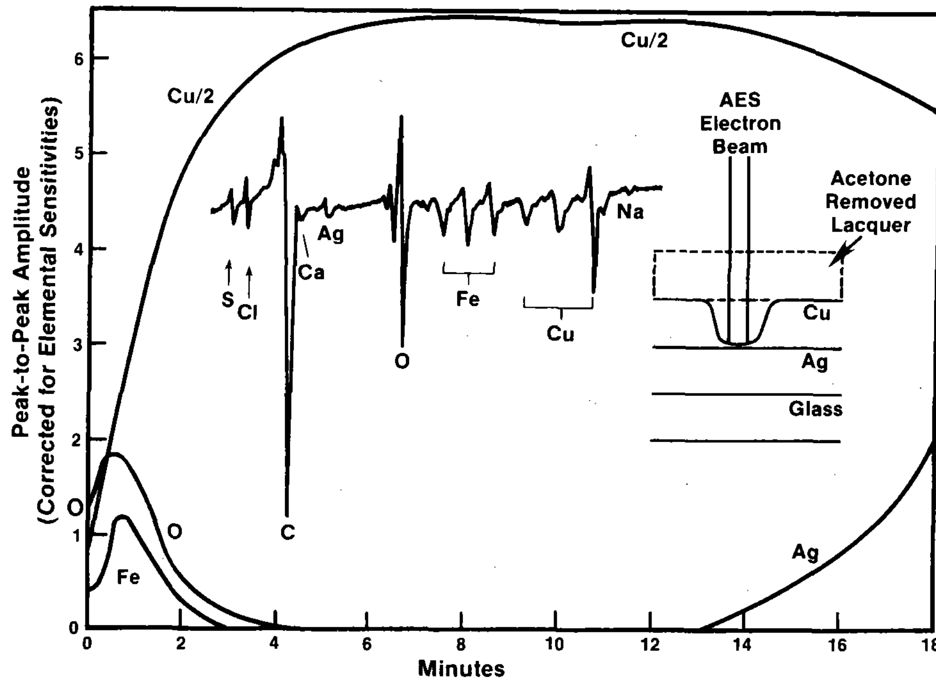

Figure 3-14. Peak to Peak Amplitude from dN(E)/dE vs. E Auger Spectra Taken during a Depth Profile through the Copper Layer of a One Year Old Mirror after Removal of a Lacquer Backing with Acetone. The Profile Has Been Corrected for Elemental Sensitivity Factors as Provided by Physical Electronics. E_p = 3 keV, I_p = 5 μA, Beam Size ~ 12 μm, E_{Ar+} = 3 keV, 1 mm × 1 mm Raster Area, I_{Ar+} = 200 nA. The Elements Present on the Copper Surface are Shown in the Inset Survey Scan Showing a Plot of dN(E)/dE vs. E (see Ref. 91).

SECTION 4.0

APPLICATIONS OF SURFACE COMPOSITIONAL ANALYSIS

The brevity of this review precludes providing illustrations of the applications of surface compositional analysis. Selected references will be provided to illustrate a few topical areas that have been studied, and it is hoped the reader will seek out examples from the thousands of papers now in the literature that apply to industrial materials science and engineering.

4.1 SURFACE MODIFICATION OF MATERIALS

Ion implantation into semiconductors has been used for over two decades to modify their semiconductor properties [66]. The in-depth distribution of the implanted species has been routinely analyzed using SIMS, AES, and RBS, depending on the concentration levels [7,12,40]. Extensive ion implantation efforts are also being carried out to modify the wear, corrosion, and erosion properties of metals and alloys. Surface compositional analysis is especially helpful for deducing the initial in-depth implant distribution and any changes that occur during annealing or applications.

4.2 SURFACE SEGREGATION AND INTERDIFFUSION

Surface segregation studies have been made for a number of alloy systems, especially of the solid solution type such as Cu-Ni [67] and for dilute alloy systems [68]. There is a surface enrichment of copper for all alloy compositions after annealing; however, sputtering and chemisorption can have significant effects on the equilibrium surface composition [67]. Experimental results obtained for sulfur or carbon segregation to single crystal nickel surfaces were consistent with those expected from theoretical predictions [68]. In this paper, J. Blakely concluded that the detailed surface structure is important for understanding the types of segregation to surfaces. Thus, the combination of compositional and structural surface analysis is important to understand this facet of materials science.

Extensive study of the interdiffusion between thin film multilayers has been made primarily with RBS techniques [40,69]. The important applications are in electronic devices; e.g., metallization contacts. AES, XPS, ISS, and SIMS analysis techniques have been applied to electronic device processing; e.g., substrate processing, deposited films, patterning, interconnects, and compatibility [70]. They have also been applied to process development and quality control [71], although SIMS and AES are preferred because of their better lateral resolution.

4.3 CORROSION

The application of AES, XPS, and RBS to corrosion problems was recently reviewed by D. Baer and M. Thomas [72]. Although the applications of these techniques is not always straightforward, their use does provide a new

dimension to understanding basic corrosion phenomena as well as the destruction of technological materials. Extensive articles where surface analysis techniques have been used can be found in Corrosion Science, Surface Technology, Applications of Surface Science, and Materials Science and Engineering.

4.4 PHOTOVOLTAIC MATERIALS AND INTERFACES

The stability of solar cells and PV materials is clearly related to interfacial phenomena, as is emphasized in a recent workshop report [73]. In this document, L. Kazmerski states the challenge lucidly; i.e.,

> . . . even a cursory examination of the cross section and microstructure of a thin-film polycrystalline solar cell can produce some skepticism in the mind of the most ardent thin-film photovoltaics advocate. How can this device, with its maze of grain boundaries, interfaces, defects, surfaces, and metallurgical junctions, be expected to remain reliable or stable even if it is allowed to remain unmolested let alone exposed to severe fields, illumination, changing loads, temperature gradients, and cycling, and its entire processing sequences.

In his research, L. Kazmerski and collaborators [74-83] have used XPS, SIMS, and high resolution (160 nm beam) SAM to resolve some of the grain boundary and interdiffusion issues in various PV cell materials, such as Si, GaAs, $CuInSe_2$, and InP. In particular, their results of the compositional studies have been correlated directly with measurement of the electron beam induced current, both made on the same region of the sample. A good overview of the technique and results was published recently [74]. The approach used is a good example of the needs for microanalytical surface studies. As the principal goals of PV research become more concerned about stability and durability rather than achieving necessary levels of performance, interface research will become increasingly important.

4.5 GLASSES

Understanding glass corrosion and controlling the technology of processing is important for many products and can be studied using compositional surface analysis. The present understanding of environmentally induced reactions at glass surfaces was recently reviewed by L. Hench and D. Clark [84]. These authors reported on using AES, XPS, and SIMS as well as other materials characterization techniques. They showed that important differences in reaction rates exist when glasses of different compositions are exposed to water vapor.

4.6 POLYMERS

Most work done on polymers has been restricted to XPS [85,86], although some studies with SIMS [86] and ISS [87] have been done [85]. Since a major problem exists with polymer degradation, XPS is ideally suited for detecting changes in the kind of functional groups covalently bonded to carbon.

Polymeric materials are crucially important to solar technologies for use as protective coatings, encapsulants, and backings for mirrors. In each of these cases, the protected material degrades when exposed to the various parameters of a solar environment.

An additional problem is that the polymer/protected-material interface may experience a degradative reaction. The protective value of the polymer may deteriorate because the UV or environmental parameters change the properties of the polymer. The copper ion catalyzed thermal oxidative degradation of polypropylene, which is discussed in technical detail in recent publications [87,88], is an example where the interface or material in the interface (e.g., copper) results in a significant catalyzed degradative reaction at lower temperatures than normal. Therefore, it is necessary to carry out studies where the synergism of UV, temperature, atmospheric gases, and the interface composition can be assessed.

One approach for studying polymers, besides using XPS [85,86], is to monitor the development of functional groups using a Fourier transform infrared spectrometer (FT-IR) fitted with an environmental test chamber (ETC) and a UV simulator, as shown in Figure 4-1. The sample in an ETC can be subjected to a flow of gases, at a controlled temperature, while being subjected to a UV flux. The IR beam is directed at the sample, and the reflected beam is focused onto the detector in the FT-IR system. The polymer of interest is

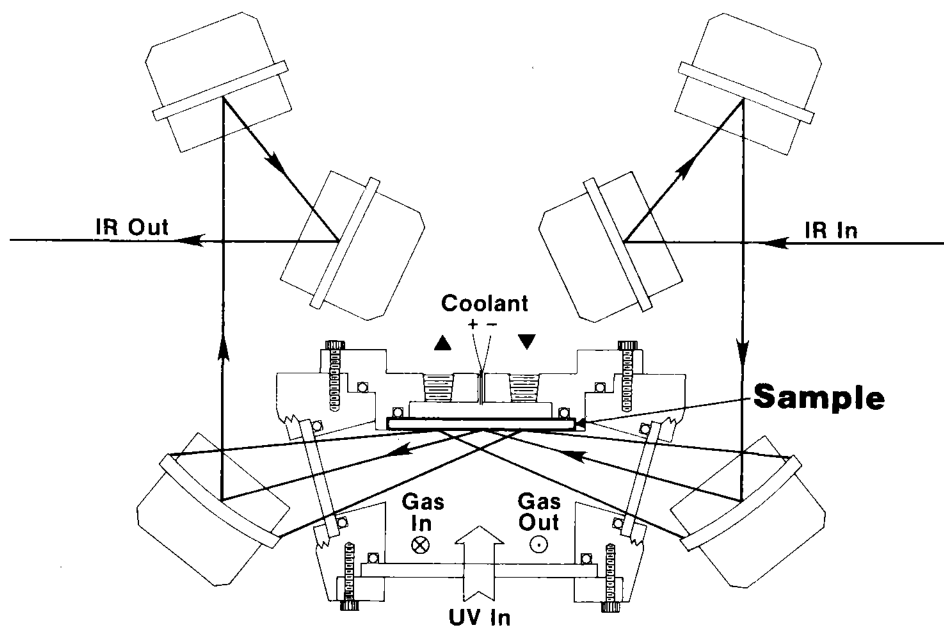

Figure 4-1. Path of Infrared Radiation through a Controlled Environmental Exposure Chamber for in situ Photodegradation of Polymeric Films on Reflecting Substrates. The Technique Is Known as Reflection-Absorptance Infra-red Spectroscopy and with a Fourier Transform Spectrometer is Defined as FT-IR-RA (see Ref. 89).

coated onto the sample; by proper selection and sequencing the study of the variables, functional groups formed in the polymer can be ascribed to UV, the polymer/metal interface, temperature, or a particular gaseous constituent. A description of the overall apparatus and initial results have been published [89]. The significance of this approach is that the simultaneous or sequential combinations of degradative parameters, which adversely affect the functional performance of the component material, can be imposed to correlate them with changes in the important mechanical, chemical, physical, and interfacial properties of the polymer.

There are other surface and interface problems related to candidate polymers for solar applications [90]. For example, the desirable transmittance of a polymer may be reduced by abrasion from the environment or the adherence of dust. The latter is primarily a problem in surface chemistry. The potential reactivity between a polymer and any other contact surface needs to be studied to determine if an interfacial incompatibility exists. Reactions at the polymer/metal interface may lead to delamination. At the same time, UV-enhanced degradation of the bulk polymer may result in adsorption of a corrosive species at the polymer/metal interface, where an undesired reaction may actually be accelerated rather than eliminated. The study of thin polymer coatings on metal and metal oxide thin films of candidate solar materials is certainly an area of broad opportunity in interface science.

4.7 SOLAR MIRRORS

Silver has the most desirable solar reflectance property of any element (~97%) and therefore will require the least concentrator area to collect a given amount of solar radiation. Although silver itself is relatively unreactive, a fractional monolayer of adsorbed oxygen enhances its reactivity to atmospheric gases, such as water, carbon dioxide, sulfur dioxide, nitric oxide, etc. At room temperature and atmospheric pressure, nearly one monolayer of oxygen always can be expected on silver. Thereore, chemisorption of atmoshperic gases initiates corrosive reactions and a degradation of the reflectance. The results of these reactions have yielded visually transparent areas in mirrors used in demonstration heliostat fields in time spans ranging from several months to a few years.

The state-of-the-art mirror system now in use is a glass, second-surface silver mirror backed with copper and paint, as shown in Figure 4-2. Interfacial degradation reactions may begin at the silver/glass interface because of impurities at the interface. These may be residual impurities resulting from the method of preparation, or the impurities may accumulate there because of radiation-induced transport processes of various ions in the glass. Deterioration of the mirror material may also result from interdiffusion of copper and silver, and reaction of the copper and then the silver with atmospheric gases. The rate of permeation of the paint backing by atmospheric gases may increase as the paint weathers in the sun and elements. For this system, the characterization and study of the glass/silver, silver/copper, and copper/paint interfaces before and after various stages of use are clearly required to understand the multilayer mirror stack shown in Figure 4-2. The ISS, XPS, AES, and SIMS methods of characterization are clearly applicable to this problem.

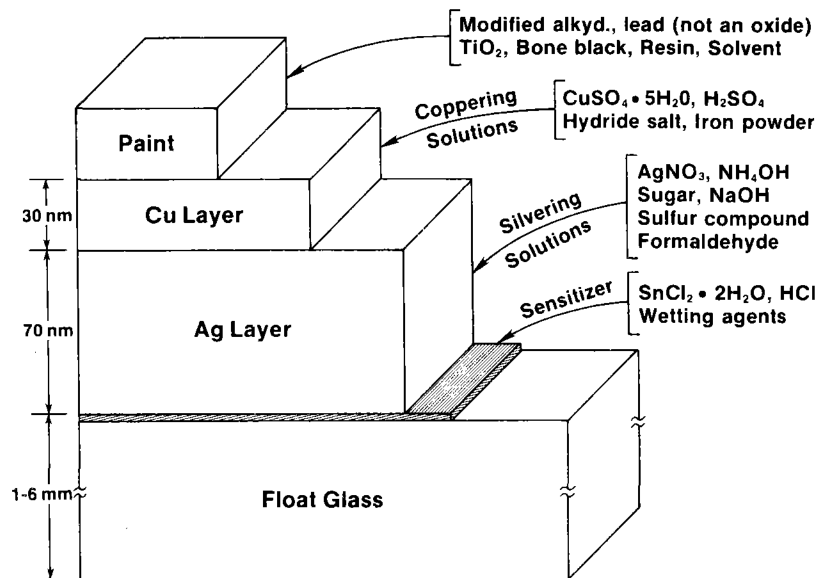

Figure 4-2. Morphology and Chemical Components Used in a Typical Commercially Made Mirror (see Ref. 91)

For solving the mirror degradation problem, it is important to prepare model mirror systems and secure commercially made mirrors now in use, and to elucidate the mechanisms of the reactions that result in deterioration of the reflectance of the mirror. Characterization of the systems should include using optical, diffraction, adhesion, and corrosion resistance measurements in addition to various methods of interface analysis (ISS, XPS, AES, SIMS, SEM, IR, etc.). Progress towards solving some of the degradation mechanisms in mirror systems of the type shown in Figure 4-2 was published recently [91].

SECTION 5.0

REFERENCES

1. H. Werner, in L. Fiermans, J. Vennik, and W. Dekeyser, (eds.), Electron and Ion Spectroscopy of Solids, Plenum, New York, 1978, p. 419.

2. C. B. Duke, in L. Casper and C. Powell, (eds.), Industrial Applications of Surface Analysis, American Chemical Society, Washington, D. C., 1982, p. 12.

3. R. W. Balluffi, G. R. Woolhouse, and Y. Komen, in H. Hu, (ed.), The Nature and Behavior of Grain Boundaries, Plenum, New York, 1972, p. 41.

4. J. O'M. Bockris, Mat. Sci. Engr., 53, 47, (1982).

5. A. W. Czanderna, J. Vac. Sci. Technol., 17, 17, (1980).

6. H. F. Winters, in M. Kaminsky, (ed.), Radiation Effects on Solid Surfaces, American Chemical Society, Washington, D. C., 1976, p. 1.

7. J. A. McHugh, in A. W. Czanderna, (ed.), Methods of Surface Analysis, Elsevier, Amsterdam, 1975, p. 229.

8. G. K. Wehner, in A. W. Czanderna, (ed.), Methods of Surface Analysis, Elsevier, Amsterdam, 1975, p. 1.

9. R. E. Honig, Thin Solid Films, 31, 89, (1976).

10. H. Werner, in L. Fiermans, J. Vennik, and W. Dekeyser, (eds.), Electron and Ion Spectroscopy of Solids, Plenum, New York, 1978, p. 324.

11. P. H. Holloway, and R. S. Bhattacharya, Mat. Sci. Engr., 52, 81, (1982).

12. J. M. Morabito, and R. K. Lewis, in A. W. Czanderna, (ed.), Methods of Surface Analysis, Elsevier, Amsterdam, 1975, p. 279.

13. A. W. Czanderna, Solar Energy Materials, 5, 349, (1981).

14. D. Lichtman, in A. W. Czanderna, (ed.), Methods of Surface Analysis, Elsevier, Amsterdam, 1975, p. 39.

15. D. Lichtman, private communication, University of Wisconsin-Milwaukee, November 1982.

16. R. F. K. Herzog, and R. P. Viehböck, Phys. Rev., 76, 855, (1949).

17. R. E. Honig, J. Appl. Phys., 29, 549, (1958).

18. A. Benninghoven, in R. Vanselow and S. Y. Tong, (eds.), Chemistry and Physics of Solid Surfaces, CRC Press, Cleveland, Ohio, 1977, p. 207.

19. G. Blaise, in J. P. Thomas and A. Cachard, (eds.), Materials Characterization Using Ion Beams, Plenum, New York, 1978, p. 143.

20. C. W. Magee, W. L. Harrington, and R. E. Honig, Rev. Sci. Instr., 49, 477 (1978).

21. C. A. Evans, Jr., Anal. Chem., 44, 67A (1972).

22. D. P. Smith, J. Appl. Phys., 38, 340 (1967).

23. D. P. Smith, Surface Sci., 25, 171 (1971).

24. H. H. Brongersma and P. M. Mul, Surface Sci., 35, 393 (1973).

25. H. H. Brongersma, J. Vac. Sci. Technol., 11, 231 (1974).

26. T. M. Buck, in A. W. Czanderna, (ed.), Methods of Surface Analysis, Elsevier, Amsterdam, 1975, p. 75.

27. E. Taglauer and W. Heiland, Appl. Phys., 9, 261 (1976).

28. G. C. Nelson, J. Colloid Inter. Sci., 55, 289 (1976).

29. E. Taglauer and W. Heiland, in T. L. Barr and L. E. Davis (eds.), Applied Surface Analysis, ASTM, Philadelphia, PA, 1980, p. 111.

30. E. Everhart, G. Stone, and R. J. Carbone, Phys. Rev., 99, 1287 (1955).

31. F. W. Bingham, Sandia Research Report, SC-RR-66-506, 1966.

32. C. A. Moyer and K. Orvek, Surface Sci., 114, 295 (1982); 121, 138 (1982).

33. T. Rusch and R. L. Erickson, in N. H. Tolk, J. C. Tully, W. Heiland, and C. W. White, (eds.), Inelastic Ion Surface Collisions, Academic, New York, 1977, p. 73.

34. R. L. Erickson and D. P. Smith, Phys. Rev. Lett., 34, 297 (1975).

35. A. W. Czanderna, A. C. Miller, H. H. G. Jellinek, and H. Kachi, J. Vac. Sci. Technol., 14, 227 (1977).

36. W. L. Baun, Appl. Surface Sci., 1, 81 (1977).

37. E. Rutherford, Phil. Mag., 21, 669 (1911).

38. H. Geiger and E. Marsden, Phil. Mag., 25, 606 (1913).

39. S. Rubin and V. K. Rasmussen, Phys. Rev., 78, 83 (1950).

40. W. K. Chu, J. W. Mayer, and M-A. Nicolet, Backscattering Spectrometry, Academic, New York, 1978.

41. L. C. Feldman, in R. C. Vanselow and W. England, (eds.), Chemistry and Physics of Solid Surfaces, Vol.3, CRC Press, Boca Raton, Florida, 1982, p. 221.

42. K. Larsson, C. Nordling, K. Siegbahn, and E. Stenhagen, Acta. Chem. Scand., 20, 2880 (1966).

43. K. Siegbahn, J. Elect. Spectros. Related Phen., 5, 3 (1974).

44. D. M. Hercules and S. H. Hercules, in P. F. Kane and G. B. Larrabee, (eds.), Characterization of Solid Surfaces, Plenum, New York, 1974, p. 307.

45. W. M. Riggs and M. J. Parker, in A. W. Czanderna, (ed.), Methods of Surface Analysis, Elsevier, Amsterdam, 1975, p. 103.

46. G. K. Wertheim, in L. Fiermans, J. Vennik, and W. Dekeyser, (eds.), Electron and Ion Spectroscopy of Solids, Plenum, New York, 1978, p. 192.

47. K. Siegbahn, et al., ESCA, Atomic Molecular and Solid State Structure Studied by Means of Electron Spectroscopy, Almqvist and Wiksells, Uppsala, Sweden, 1967.

48. K. Siegbahn, ESCA Applied to Free Molecules, Elsevier, New York, 1971.

49. T. A. Carlson, Photoelectron and Auger Spectroscopy, Plenum, New York, 1975.

50. C. R. Brundle and A. D. Baker, (eds.), Electron Spectroscopy: Theory, Techniques, and Applications, Academic, London, Vol. 1, 1977; Vols. 2, 3, and 4, 1978.

51. J. H. Scofield, J. Electron Spectr., 8, 129 (1976).

52. S. Evans, R. G. Pritchard, and J. M. Thomas, J. Electron Spectr., 14, 341 (1978).

53. C. J. Powell, in N. S. McIntyre, (ed.), Quantitative Surface Analysis of Materials, ASTM, STP 643, Philadelphia, PA, 1978, p. 5.

54. P. Auger, J. Phys. Radium, 6, 205 (1925).

55. J. J. Lander, Phys. Rev., 91, 1382 (1953).

56. L. A. Harris, J. Appl. Phys., 39, 1419 (1968).

57. P. W. Palmberg, in G. A. Somorjai, (ed.), The Structure and Chemistry of Solid Surfaces, Wiley, New York, 1968, p. 29-1.

58. D. E. Stein, R. E. Weber, and P. W. Palmberg, J. Metals, 23, 39 (1971).

59. C. C. Chang, Surface Sci., 25, 53 (1971); also in P. F. Kane and G. B. Larrabee, (eds.), Characterization of Solid Surfaces, Plenum, New York, 1974, p. 509.

60. E. N. Sickafus and H. P. Bonzel, in E. Danielli, R. Rosenberg, and D. Cadenhead, (eds.), Progress in Surface and Membrane Science, Vol. 4, Academic, New York, 1971, p. 1.

61. T. E. Gallon and J. A. D. Matthew, Rev. Phys. Technol., 3, 31 (1972).

62. J. C. Rievere, Contemp. Phys., 14, 513 (1973).

63. A. Joshi, L. E. Davis,and P. W. Palmberg, in A. W. Czanderna, (ed.), Methods of Surface Analysis, Elsevier, Amsterdam, 1975, p. 218.

64. G. Ertl and J. Kuppers, Low Energy Electrons and Surface Chemistry, Verlag Chemie, Weinheim, FRG, 1974.

65. C. D. Wagner, Faraday Disc., 60, 291 (1975).

66. J. W. Mayer, L. Eriksson, and J. A. Davies, Ion Implantation in Semiconductors, Academic, New York, 1970.

67. D. T. Ling, I. Lindau, J. N. Miller, and W. E. Spicer, in T. L. Barr and L. E. Davis, (eds.), Applied Surface Analysis, ASTM, STP 699, Philadelphia, PA, 1980, p. 66.

68. J. Blakely, in R. Vanselow, (ed.), Chemistry and Physics of Solid Surfaces, Vol. 2, CRC Press, Cleveland, Ohio, 1979, p. 237.

69. J. M. Poate, K. N. Tu, and J. W. Mayer, (eds.), Thin Films - Interdiffusion and Reactions, Wiley, New York, 1978.

70. P. Holloway, in T. L. Barr and L. E. Davis, (eds.), Applied Surface Analysis, ASTM, STP 699, Philadelphia, PA, 1980, p. 5.

71. M. A. Ryan and G. E. McGuire, in L. A. Casper and C. J. Powell, (eds.), Industrial Applications of Surface Analysis, American Chemical Society, Washington, C. B., 1982, p. 229.

72. D. R. Baer and M. T. Thomas, in L. A. Casper and C. J. Powell, (eds.), Industrial Applications of Surface Analysis, American Chemical Society, Washington, D. C., 1982, p. 251.

73. D. E. Sawyer and H. A. Schafft, (eds.), Stability of (Thin Film) Solar Cell Materials, NBS Special Publication 400-58, U. S. Dept. of Commerce, Washington, D. C., August, 1979.

74. L. L. Kazmerski, Applied Surface Sci., 7, 55, (1981).

75. L. L. Kazmerski, P. J. Ireland, and T. F. Ciszek, Appl. Phys. Lett., 36, 323 (1980).

76. L. L. Kazmerski, in A. Benninghoven, C. A. Evans, R. A. Powell, R. Shinizu, and H. A. Storms, (eds.), Secondary Ion Mass Spectroscopy - SIMS II, Springer-Verlag, New York, 1980, p. 83.

77. L. L. Kazmerski and P. J. Ireland, J. Vac. Sci. Technol., 17, 525 (1980).

78. L. L. Kazmerski, P. J. Ireland and P. Sheldon, Proc. 14th IEEE Photovoltaic Spec. Conf.-San Diego, IEEE, New York, 1980, p. 1311.

79. L. L. Kazmerski, P. Sheldon and P. J. Ireland, Thin Solid Films, 58, 95 (1979).

80. T. L. Chu, S. S. Chu, L. L. Kazmerski, R. L. Whitney, C. L. Lin and R. M. Davis, Solar Cells, 5, 388 (1981).

81. L. L. Kazmerski, in H. Windawi, (ed.), Applied ESCA, Wiley, New York, 1981, p. 48.

82. L. L. Kazmerski, P. J. Ireland, P. Sheldon, T. L. Chu, S. S. Chu and C. L. Lin, J. Vac. Sci. Technol., 17, 1061 (1980).

83. L. L. Kazmerski, P. J. Ireland, O. Jamjoum and R. L. Whitney, J. Vac. Sci. Technol., 18, 960 (1981).

84. L. L. Hench and D. E. Clark, in L. A. Casper and C. J. Powell, (eds.), Industrial Applications of Surface Analysis, American Chemical Society, Washington, D. C., 1982, p. 203.

85. D. T. Clark, in R. Vanselow, (ed.), Chemistry and Physics of Solid Surfaces, Vol. 2, CRC Press, Cleveland, Ohio, 1979, p. 305.

86. D. W. Dwight, T. J. Fabish, and H. R. Thomas, (eds.), Photon, Electron, and Ion Probes of Polymer Structure and Properties, American Chemical Society, Washington, D. C., 1981.

87. A. C. Miller, A. W. Czanderna, H. H. G. Jellinek, and H. Kachi, J. Colloid Interface Sci., 85, 244 (1982).

88. H. H. G. Jellinek, H. Kachi, A. W. Czanderna and A. C. Miller, J. Polymer Sci., 17, 1493 (1979) and references cited therein.

89. J. D. Webb, D. M. Smith, A. Chughtai, P. Schissel, and A. W. Czanderna, Appl. Spectros., 35, 598 (1981).

90. W. Carroll and P. Schissel, Polymers in Solar Technologies: an R and D Strategy, SERI/TP-641-601 (Solar Energy Research Institute, Golden, CO, USA, July 1980) available from NTIS.

91. T. M. Thomas, J. R. Pitts, and A. W. Czanderna, Appl. Surface Sci., 15, 75 (1983).

Document Control Page	1. SERI Report No. SERI/TR-255-2217	2. NTIS Accession No.	3. Recipient's Accession No.

4. Title and Subtitle
Materials Characterization Using Ion, Electron, and Photon Probes

5. Publication Date
May 1984

6.

7. Author(s)
A. W. Czanderna

8. Performing Organization Rept. No.

9. Performing Organization Name and Address
Solar Energy Research Institute
1617 Cole Boulevard
Golden, Colorado 80401

10. Project/Task/Work Unit No.
1064.10

11. Contract (C) or Grant (G) No.
(C)
(G)

12. Sponsoring Organization Name and Address

13. Type of Report & Period Covered
Technical Report

14.

15. Supplementary Notes

16. Abstract (Limit: 200 words) The content of a lecture at the senior-graduate level on materials characterization using ion, electron, and ion probes is amplified and extensively referenced. The emphasis of the report is compositional surface analysis using secondary ion mass spectrometry (SIMS), ion scattering spectrometry (ISS), Rutherford backscattering spectrometry (RBS), x-ray photoelectron spectroscopy (XPS), and Auger electron spectroscopy (AES). The physical principles, experimental methods, advantages and limitations, and illustrative examples for each of the five methods are discussed. Composition in depth profiling using sputter ion etching is also described, including mechanisms, yields, rates, instrumentation, advantages, and limitations. Brief comments and literature citations are given for materials characterization using SIMS, ISS, RBS, AES, and XPS in corrosion, surface modification, surface segregration, thin films, and grain boundaries for various materials of interest in industrial materials science and engineering. Extensive references are provided as a guide for those desiring greater depth in the topical areas discussed.

17. Document Analysis

a. Descriptors Electron Microprobe Analysis ; Electron Probes ; Ion Microprobe Analysis Mass Spectroscopy ; Microanalysis ; Surfaces

b. Identifiers/Open-Ended Terms

c. UC Categories

59 , 61c, 62 , 63d,e, 64

18. Availability Statement
National Technical Information Service
U.S. Department of Commerce
5285 Port Royal Road
Springfield, Virginia 22161

19. No. of Pages
53

20. Price
A04

Form No. 0069 (3-25-82)

United States Department of Energy
Office of Scientific and Technical Information
Post Office Box 62
Oak Ridge, Tennessee 37831

OFFICIAL BUSINESS
PENALTY FOR PRIVATE USE, $300

POSTAGE AND FEES PAID
DEPARTMENT OF ENERGY
DOE-350

689 FS- 1
SANDIA NATIONAL LABS
ATTN A C SKINROOD
DIVISION 8452
LIVERMORE, CA 94550